UNIVERSITÀ degli STUDI di CATANIA
Dipartimento di Agricoltura, Alimentazione e Ambiente
Di3A

UNIVERSITÀ DEGLI STUDI DI CATANIA

INTERNATIONAL PHD COURSE IN
"AGRICULTURE, FOOD AND ENVIRONMENTAL SCIENCE" XXIX CYCLE

Monitoring and modeling fluxes transfer processes in soil-plant-atmosphere *continuum* across scales

Daniela Vanella

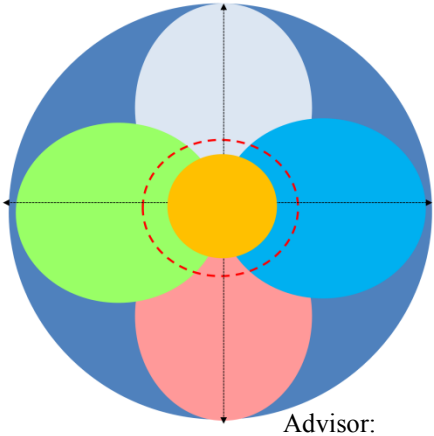

Advisor:
Prof. Simona Consoli

Coordinator:
Prof. Cherubino Leonardi

PhD attended during 2013/2016

Table of contents

List of figures

List of tables

Abbreviations and symbols

°C	Celsius degree
1D	one-dimensional
3D	three-dimensional
α	regularization parameter
α’	constants in the water retention van Genuchten model (1980)
a	correction coefficient derived by Swanson and Whitfield (1981)
ACM	Citrus and Mediterranean Crops Research Centre
b	correction coefficient derived by Swanson and Whitfield (1981)
c	correction coefficient derived by Swanson and Whitfield (1981)
c’	scalar concentration fluctuations
C1	first quarter treatment T1
C2	second quarter treatment T1
C3	third quarter treatment T1
C4	fourth quarter treatment T1
CREA	Italian Council for Agricultural Research and Agricultural Economics Analyses
c_p	specific heat of air at a constant pressure
CZ	critical zone
d	data (measured apparent resistivity)
d_i	measurement data vector
d_r	resistance ratio
d_0	dataset collect at the initial condition
d_t	data collected at time (t)
DC	direct current
D_T	displacement of water
ε	data error
Δm	parameter update
ΔT	temperature variation
EC	eddy covariance

EM	electromagnetic induction
ER	electrical resistivity
ERT	electrical resistivity tomography
ERT1	first ERT monitoring 2015
ERT2	second ERT monitoring 2015
ERT3	third ERT monitoring 2015
ET_0	reference evapotranspiration
ET	evapotranspiration
FDR	frequency domain reflectometry
F_m	forward model
F_M	volume fractions of wood
F_L	volume fractions of water
G	soil heat flux
GPR	ground-penetrating radar
H	sensible heat flux
h	radius
h_c	canopy height
HPV	heat pulse velocity
J	Jacobian (or sensitivity) matrix
j	sap flux density
k	iteration
K	geometric factor
K(h)	soil hydraulic conductivity tensor
K_c	crop coefficient
K_s	hydraulic conductivity at saturation
λ	latent heat of vaporization
λE	latent heat flux
LAI	leaf area index
LT	local time
m	model parameter
m’	constants in the water retention van Genuchten model (1980)
M_D	mass of dry wood
M_F	mass of fresh wood
M_L	mass of water
n	constants in the water retention van Genuchten model (1980)

N	number of measurements
PAR	photosynthetic active radiation
pF	retention curve
PRD	partial root-zone drying
q’	concentration of the transported water vapour
Q1	first quarter treatment T4
Q2	second quarter treatment T4
Q3	third quarter treatment T4
Q4	fourth quarter treatment T4
SIAS	Agro-meteorological Service of the Sicilian Region
SP	soil-plant
SPAC	soil-plant-atmosphere *continuum*
SWC	soil water content
ρ_a	apparent resistivity
ρ_m	calculated resistivity
ρ_{air}	air density
ρ	electrical resistivity
ρ_L	water density
ρ_M	density of dry wood
R	roughness matrix
r	stem radius
RMS	root mean square misfit
RN	net radiation
RS	remote sensing
RWU	root water uptake
S	sink source term
θ	volumetric soil water content
θ_r	residual water content
θ_s	saturated water content
t	time
T	temperature
T1	full irrigation treatment
T4	deficit irrigation treatment
TDR	time-domain reflectometry
T_{SF}	transpiration
t_z	time delay

V_c	corrected heat pulse velocity
V_T	total volume
V_z	raw heat pulse velocity
w’	vertical velocity fluctuations
W_d	data weight matrix
WPL	Webb, Pearman, Leuning
X_u	upstream distance below the heater
X_d	downstream distance above the heater
Ψ_d	objective function
Ψ_m	model penalty term

Acknowledgements

The pages of this manuscript are the work of many minds and hands that I have been lucky to meet during the PhD years.

My best thanks are to my Advisor – prof. Simona Consoli - for all the guidance and opportunities that she gave me during the PhD period.

I wish to thank the components of hydraulic research group of the Department of Agriculture, Food and Environment (DI3A), University of Catania - prof. Salvatore Barbagallo, prof. Giuseppe Cirelli, dr. Rosa Aiello, dr. Feliciana Licciardello - for welcoming me into a "research family".

I really thank the members of geophysics research group of the Department of Geoscience, Padua University - prof. Giorgio Cassiani, dr. Jacopo Boaga, dr. Maria Teresa Perri, dr. Laura Busato - for the intense collaboration that we have built in these years, their huge assistance in the geophysical experimental design.

I am sincerely grateful to prof. Andrew Binley for the precious teachings and recommendation on the use of hydro-geophysics techniques and for his twice hospitality at the Lancaster Environment Centre (LEC) of Lancaster University (UK).

I wish to thank dr. Giovanni Zocco and dr. Alessandro Castorina for their help during the geophysical monitoring fieldwork in 2015.

Moreover, I wish to thank the personnel of the Citrus and Mediterranean Crops Research Centre of the Italian Council for Agricultural Research and Agricultural Economics Analyses (CREA-ACM, Acireale) and especially dr. Giancarlo Roccuzzo and dr. Fiorella Stagno for their support in the research activity.

Without the help of all these people, this thesis would never have come into existence. Now I wish you an enjoyable travel through the pages of this manuscript.

Preface

Complex exchange processes characterize the soil, vegetation and the lower atmosphere system. While the exchange of mass (mainly water and carbon) and energy is continuous between these compartments, the pertinent transfer fluxes are strongly heterogeneous and variable in space and time.

Within the soil-plant-atmosphere *continuum* (SPAC) system, root activity plays a crucial role because it connects different domains and allows the necessary water and nutrient exchanges for plant growth. Plant roots have a major role in mass and energy exchanges between soil and atmosphere.

Yet, monitoring the activity of the root-zone is a challenge as roots are not visible from the soil surface and they evolve in space and time responding to internal and external forcing conditions. Therefore, devising strategies that can provide insight into the activity of roots have an impact both on practical activities such as precision agriculture and on answering large-scale questions e.g. related to climatic change.

The comprehension of the mass exchange dynamics within the SPAC is useful not only for eco-hydrological purposes, by contributing to the understanding of the critical zone (CZ) dynamics (Jayawickrem et al., 2014; Parsekian et al., 2015), but also plays a central role in the definition of precision agriculture criteria, especially when an optimisation of water resources exploitation is mandatory.

The PhD thesis is organized into five Chapters.

The first Chapter contains both an introduction on the general concepts, based on the research motivations, and a summary of the main objectives of the PhD work.

The second Chapter presents a theoretical insight on the methodological approaches adopted during the experimental campaigns.

The third and fourth Chapters systematically describe two experimental Case study applications. Each of these Chapters includes a description of the field site and the materials and methods, the achieved results and discussions.

Summary and conclusions are in the fifth Chapter.

Abstract

The soil-plant-atmosphere (SPA) interactions are a critical component of the Earth's biosphere because of their crucial role in the hydrological cycle. For a better understanding of the functional interactions between natural resources and related sustainability problems, the scientific community is becoming aware that more interdisciplinary approaches are required.

Understanding SPA processes and principally root-zone uptake (RWU) is actually significant for proper irrigation management especially in areas characterized by scarce water availability, such as the Mediterranean areas. Such understanding requires an ability to map the hydrological dynamics at high spatial and temporal resolution and appropriate scale.

The PhD work encourage at using innovative and advanced techniques to monitor the exchanges of mass and energy within the soil-plant-atmosphere continuum (SPAC) at different spatial scales.

The novelty of the PhD work is the assimilation of geophysical data with other more conventional measurements (micrometeorogical and transpiration data) in order to interpret some of the principal transfer processes acting through the SPAC (i.e., evapotranspiration and RWU) in semi-arid climate.

The PhD thesis covers two cases studies looking at the use of an integrated approach to help unravel the complexity of soil-plant interactions, specifically concerning RWU of citrus trees.

In the first Case study, electrical imaging, sap flow data, eddy covariance measurements and modelling were coupled to determine the RWU area of an orange tree.

The second Case study, explores RWU patterns of orange trees under different irrigation schedules, by integrating small scale 3D electrical resistivity tomography (ERT) with sap flow measurements.

Results have demonstrated the ability of electrical imaging techniques to link the soil moisture distribution with crop physiological response (i.e. transpiration fluxes) and the active root distribution in the soil, thus providing new insight into the use of geophysical measurements.

Sommario

Alle interazioni tra le diverse componenti del sistema suolo-pianta-atmosfera (SPA) è attribuito un ruolo critico nel ciclo idrologico e della biosfera terrestre.

La comunità scientifica specializzata è sempre più consapevole della necessità di portare avanti studi a carattere interdisciplinare per la comprensione delle interazioni funzionali tra le risorse naturali ed i relativi problemi di sostenibilità del sistema SPA.

All'interno di tali studi interdisciplinari, l'analisi delle interazioni suolo-radice risulta rilevante anche per la gestione ottimale dell'irrigazione, in particolare nelle zone caratterizzate da scarsa disponibilità idrica, come le aree mediterranee. A tal fine nasce l'esigenza di valutare, ad alta risoluzione sia spaziale che temporale, le dinamiche idrologiche del sistema SPA, sino alla scala dell'apparato radicale.

Il contributo della tesi di dottorato consiste nell'applicazione di tecniche di monitoraggio avanzate e minimamente invasive, per valutare gli scambi di massa ed energia all'interno del sistema SPA.

L'aspetto innovativo del lavoro di tesi consiste nell'integrazione di tecniche geofisiche con misure micrometeorologiche e dati di traspirazione, al fine di interpretare alcuni dei principali processi di trasferimento di

flussi nel sistema SPA (evapotraspirazione ed assorbimento radicale) in ambiente semi-arido.

Tale approccio, è stato applicato a due Casi studio con l'obiettivo di monitorare le complesse interazioni del sistema suolo-pianta, con particolare riferimento al processo di assorbimento radicale di alberi di agrume.

Nel primo Caso studio, la tecnica della tomografia di resistività elettrica (ERT) tridimensionale è stata integrata con dati di traspirazione, misure micrometeorologiche e modellistica idrologica al fine di delineare la porzione di suolo non satura interessata dalle radici attive di un aranceto adulto.

Nel secondo Caso studio, il monitoraggio ERT è stato integrato con misure di traspirazione al fine di delineare i pattern di RWU di alberi di arancio irrigati in regime di deficit.

I risultati del lavoro di tesi dimostrano l'abilità della tecnica di monitoraggio geofisico ERT nello spiegare le dinamiche idriche del suolo e la risposta fisiologica della pianta, in termini di attività delle radici nel processo di uptake, contribuendo, in tal senso, a migliorare la conoscenza dei processi di assorbimento radicale.

Chapter 1

Introduction

Introduction

1.1 The soil-plant-atmosphere relationship

The "critical zone" (CZ) is the breathing skin of Earth: a life-supporting epidermis that reaches from the top of vegetation down through soil and bedrock (Parsekian et al., 2015). Starting from this definition, soil and water are two critical components of the Earth's CZ. A schematic of CZ components is given in Figure 1.1.

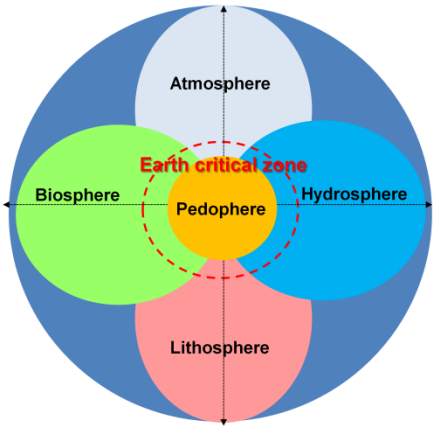

Figure 1.1 A schematic of the critical zone (CZ) components (modified from Wilding & Lin, 2006; Du & Zhou, 2009)

In general, soil modulates the connection between bedrock and atmospheric boundary layer and water is a major driving force and transport agent between these two compartments. The interactions between soil and water are so close and complex that cannot be effectively studied by stand-alone approaches. They require a system approach. The pedosphere as defined by Du & Zhou, (2009) is the thin skin of soil on the Earth's surface that represents a geomembrane across which water and solutes, as well as energy, gases, solids, and organisms are actively exchanged with the atmosphere, biosphere, hydrosphere, and lithosphere to create a life-sustaining environment. Soil–water interactions create the fundamental interface between the biotic and abiotic and hence serve as a critical determinant of the state of the Earth system and its critical zone (Wilding & Lin, 2006).

In recent years, authors (Lin, 2010 and references inside) have demonstrated that interdisciplinary approaches have significance in advancing both soil science and hydrology and can guide more effective field data acquisition, knowledge sharing, model-based prediction of complex scenario and soil-plant-atmosphere *continuum* (SPAC) relationships across scales. John R. Philip pioneered the concept of SPAC, as follows: "Because water is generally free to move across the plant-soil, soil-atmosphere, and plant-atmosphere interfaces it is necessary and desirable to view the water transfer system in the three domains of soil, plant, and atmosphere as a whole ...it must be pointed out that, as well as serving as a vehicle for water transfer, the SPAC is also a region of energy transfer" (Philip, 1966).

In this spirit, the synergistic integration of soil and life science in combination with hydrology can offer a renewed perspective and an integrated approach to understanding interactive soil and water processes and their properties in the CZ (Lin et al., 2015; Lin et al., 2003). As expected from the above description, the unsaturated soil is a complex system governed by greater non-linear processes and interactions. The SPAC systems that cover the lands of our Earth are the Earth's CZs, providing valuable ecosystem services (NRC, 2004). Through these systems, there are massive fluxes and storages of mass (water and carbon) and energy, and these provide both valuable productive and ecosystem goods and services.

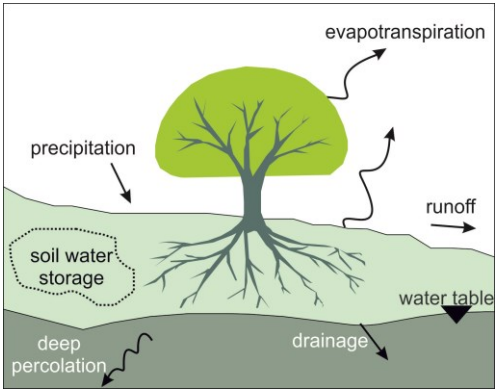

Figure 1.2 Water balance at the plant scale

Progress has achieved in advancing scientific knowledge on the SPAC and understanding the controls on hydrologic fluxes as well as how these controls vary spatially and temporally with scale (e.g., Cammalleri et al., 2013; Cassiani

et al., 2015; Consoli & Vanella, 2014 a and b; Minacapilli et al., 2016). At larger scale, crops affect the terrestrial water cycle and underground water dynamics through evapotranspiration (ET) and root water uptake (RWU), respectively. An overview of the principal hydrological processes acting within the SPAC at the small scale is shown in Figure 1.2. It is therefore not surprising that the understanding of water flow processes taking place in the SPAC has been a popular research topic during the second half of the 20th and beginning of the 21st century.

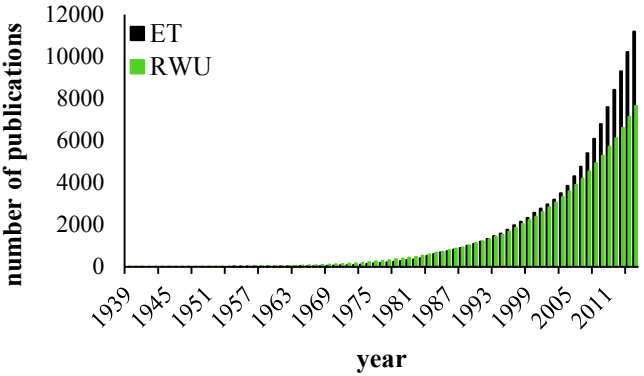

Figure 1.3 Comparison between the number of publications including 'root water uptake' and 'evapotranspiration' within 1939 and 2015 from Scopus (data not normalized respect to the total number of publications)

The graph in Figure 1.3 reports a comparison between the number of publications with title, abstract or key words containing 'root water uptake' and 'evapotranspiration' within 1939 and 2015, limiting the search to the "agriculture"

subject area (Source: Scopus, https://www.scopus.com). At the end of the year 2015 the publications containing the words "evapotranspiration" or "root water uptake", with the characteristics described above, were 11191 and 7667, respectively; with an increment of about 65 and 53% in last ten years, respectively.

1.2 Root water uptake models

In this paragraph, there is a summary on the state-of-the-art about modelling and estimates of root water uptake (RWU).

The translation of water use strategies by crops into physically based models of RWU is a crucial issue in eco-hydrology and no agreement exists on the modelling of this process (Feddes et al., 2001; Raats, 2007). The mechanisms of water transport within unsaturated soil layers in the root-zone are mainly controlled by soil physics, plant physiology and meteorological factors (Green et al., 2003a). Today there is a general accord on the tension-cohesion theory to describe the ascent of water in plants. This theory states that the water is passively extracted from the soil and flows to the atmosphere through the plant. The "catenary hypothesis" (van den Honert, 1948) is largely considered as a valid concept to modelling water flow in roots. Water is transported within the SPAC that is principally controlled by the resistances as determined by the rhizosphere, the cortex, the xylem and between the leaves and the atmosphere through the stomata. Resistances in SPAC are generally a function of the plant basic anatomy, development and metabolism; and they are all potentially variable in time and space (Hose et al., 2000;

Carminati and Vetterlein, 2012). Some resistances such as those stomata are also variable depending on plant responses and environmental effects (Blum, 2011). Therefore, the quantification of resistances to water flow along the pathway between the plant and the atmosphere is still the subject of extensive researches. Javaux et al., (2013) report that nowadays measurements of local resistances are still hardly achievable or their determination is still prone to large uncertainty. The uncertainty concerning the magnitude and location of resistances led in the past to simplifying sometimes-simplistic modelling approaches for RWU.

Typically, RWU is accounted for the Richards' equation with a sink source term, S [L^3 L^{-3} T^{-1}]:

$$\frac{\delta\theta}{\delta t} = \nabla\left(\mathrm{K(h)}\nabla h\right) + \frac{\delta \mathrm{K(h)}}{\delta z} + S \qquad (1.1)$$

where θ denotes the volumetric soil water content [L^3 L^{-3}], t the time [T], z the vertical coordinate [L], K(h) the soil hydraulic conductivity tensor [L T^{-1}]. In the right-hand of the Eq (1.1), the two terms describe the water flow redistribution between layers or soil locations, while the third one describes the water uptake by plant roots (S<0) or root exudation (S>0).

From a conceptual point of view, two main approaches exist today to predict the volumetric rate of RWU in volume elements of soil (Javaux et al., 2013). On the one hand, physically based models may explicitly consider the three-dimensional distribution of the root system together with a

distribution of the system conductances at plant scale (Doussan et al., 2006; Schneider et al., 2010).

The major limitation of this kind of models is the cost for characterizing parameters, such as root system architecture, conductance to water flow, etc, and the fact that it is very demanding in terms of computational power and time. On the other hand, effective models exist that represent the uptake behaviour at the plant scale through "macroscopic parameters". In the macroscopic approach, the sink term is typically composed of four terms that affect the magnitude and spatiotemporal dynamics of RWU, such as:

- the root hydraulic resistance distribution;
- the soil hydraulic resistance;
- a stress function describing the plant answer to an excessive climatic demand of water;
- a compensation function (Jarvis, 1989) representing the impact of the water potential distribution inside plant xylem vessels for the distribution of water uptake from the soil profile.

In three-dimensional models, the two first variables are explicitly considering accounting for the distribution on the root architecture and the root and hydraulic proprieties (potentially changing in time). The third variable is defined by a function of the water potential in the leaf. The fourth variable arises from the solution of the flow equations that are coupled between the root and the soil systems. These functions are usually simple, with few parameters and easy to

compute, but some of their parameters need calibration, which introduces uncertainties (Musters and Bouten, 2000). The RWU modelling complexity is highly related to the irregular root distribution in the vertical and radial directions (Gong et al., 2006). This variability is also induced by uneven soil layers, water and nutrient distribution and the localized soil compaction, caused by both cultivation patterns and frequent irrigation (Jones and Tardieu, 1998).

Therefore, it is evident the need to continue the development of RWU modelling approaches by increasingly the accuracy and completeness of the existing approaches (Feddes et al., 2001; Raats, 2007; Jarvis, 2011; Couvreur et al., 2012), and also integrating them with highly accurate measurements techniques of RWU activity proxy such as monitoring of soil moisture in the root-zone.

1.3 Hydro-geophysics approach

As introduced above, soil moisture measurements (Figure 1.4) may be paramount to implement RWU models. Traditionally beneath irrigated crops, soil moisture measurements have been determined using point or local measurement methods (Romano, 2014). There are numerous well-accepted methods for measuring soil moisture such as: gravimetric technique, dielectric methods (e.g., time-domain reflectometry, TDR; frequency-domain reflectometry, FDR), capacitance probe, neutron probe techniques.

The advantage of these methods is their robustness, but obviously, they suffer of limited spatial coverage. It is often

impractical obtain the number of measurements necessary to achieve a good spatial resolution. Furthermore, most of the traditional techniques are invasive and may disturb the *in situ* moisture distribution that is required from the measurement.

Robinson et al. (2008) report that contact free measurement techniques, such as remote sensing (RS) methods including passive microwave radiometers, are prominent in this category. These approaches are either ground based or operated from airborne or space borne platforms. Key limitations of current RS methods are problems with spatial averaging and a small penetration depth.

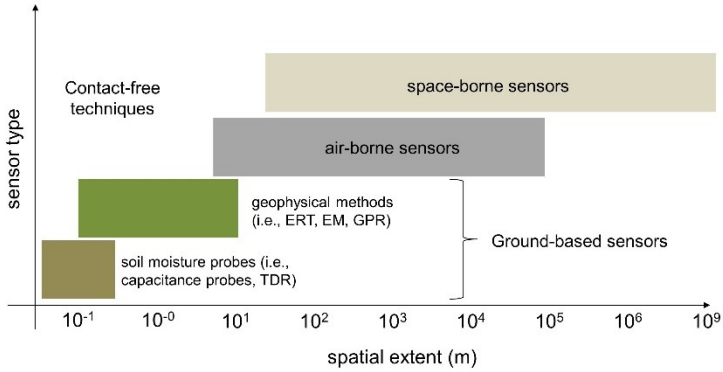

Figure 1.4 Soil moisture measurements obtained by ground-based sensors and contact-free techniques (modified from Vereecken et al., 2008)

Contact-free hydro-geophysical methods are also increasingly used (Vereecken et al., 2008). The past twenty years, in particular, have seen the fast development of geophysical techniques that are useful in identifying structure

and dynamics of the near surface, such as soil moisture distribution, with particular reference to hydrological applications. This realm of research goes under the general name of hydro-geophysics (Rubin et Hubbard, 2005, Vereecken et al., 2006, Binley et al., 2011; Binley et al., 2015a) and covers a wide range of applications and different spatial scales, from flow and transport in aquifers (e.g.,. Kemna et al., 2002; Perri et al., 2012) to the vadose zone (e.g. Daily et al., 1992, Müller et al., 2010; Oberdörster et al., 2010) (Figure 1.5).

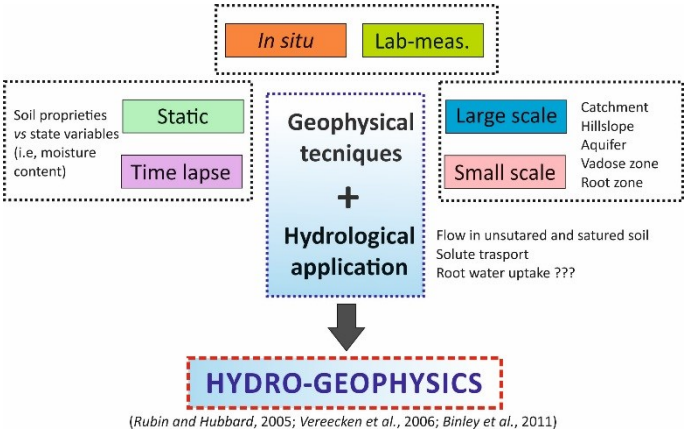

Figure 1.5 Conceptual model of the hydro-geophysics application (Rubin and Hubbard, 2005, Vereecken et al., 2006, Binley et al., 2011)

Authors have demonstrated how especially electrical geophysical methods can successfully image moisture dynamics in both field and laboratory (Koestel et al., 2008) settings. These methods can provide spatially continuous

information, thus avoiding the need for interpolation between sparsely distributed point-based measurements. For example, moisture fronts following natural rainfall events have been imaged by electrical resistivity imaging (Zhou, ey al., 2001; Binley et al., 2002; Robinson et al., 2012a; Schwartz et al.,2008), supported by laboratory experiments to determine appropriate pedophysical relationships to convert resistivity changes to changes in the distribution of moisture content.

Such studies have conclusively demonstrated that surface-electrical resistivity is a viable method for monitoring and defining vadose zone transport parameters and redistribution processes (Robinson et al., 2012). Generally, electrical resistivity can be related to soil state variables (such as soil moisture and salt concentration) and properties (clay content) and as well root properties, such as root mass (Amato et al., 2008; Paglis, 2013; Rossi et al. 2011).

Time-lapse geophysical measurements may be used to monitor spatial patterns of dynamic processes like water flow, root water uptake, and/or solute transport in soils in agricultural contexts (for details see, paragraph 2.1).

Relatively numerous hydro-geophysical applications, though, have been focussed on plant root system characterization (e.g. al Hagrey, 2007; al Hagrey and Petersen, 2011; Javaux et al., 2008; Jayawickreme et al., 2008; Werban et al., 2008), often limiting the analysis to a tentative identification of the main root location and extent.

As mentioned above, electrical soil properties are a clear indication of soil moisture content distribution, and electrical

and electromagnetic methods have been used to identify the effect of root activity (e.g. Cassiani et al., 2012; Shanahan et al., 2015). In particular, electrical resistivity tomography (ERT) has been used to characterize RWU and root systems (Garré et al., 2011; Michot et al., 2001, 2003; Srayeddin and Doussan, 2009). Amato et al. (2009, 2010) tested the ability of 3-D ERT for quantifying root biomass on herbaceous plants. Beff et al. (2013) used 3-D ERT for monitoring soil water content in a maize field during late growing seasons. Boaga et al. (2013) and Cassiani et al. (2015) demonstrated the reliability of the method respectively in apple and orange orchards. These works provide useful and promising insights into the application of the hydro-geophysical approach for the SP system characterization.

1.4 Objectives

The main objectives of the PhD work are: (i) to evaluate a new approach to understanding SPAC dynamics across space and time and (ii) to explore synergistic efforts from soil science and hydrology, along with other related disciplines such as hydro-geophysics, micrometeorology and life science.

Herein, different methodologies were coupled (e.g., geophysical methods, sap flow techniques, micro-meteorological approaches) with the main purpose of improve our understanding on the effect of soil-root interface on water dynamics.

The practical goal of the study is to identify RWU patterns of irrigated citrus trees in Mediterranean environment, also

under deficit irrigation strategy. From a methodological viewpoint, the specific goals of my PhD work are:

– studying the feasibility of root-zone monitoring by time-lapse 3-D electrical resistivity tomography (ERT) at small (decametric) scale,

– improving the identification of root-zone water dynamics by integrating ERT with transpiration sap flow data,

– interpreting ERT data with the aid of a physical hydrological model, in order to derive information on the root-zone physical structure and its dynamics,

– assessing the value of ERT data for a qualitative description of SPAC interactions in different irrigation treatments (full and deficit irrigation).

Chapter 2

Methodological approaches

Methodological approaches

2.1. Overview of geophysical methods applied to agriculture

Geophysical methods have been becoming an increasingly valuable tool for application within a variety of agro-ecosystems (Table 2.1).

Geophysical methods, such as electromagnetism, ground penetrating radar, electrical resistivity, do not affect the soil structure and the resulting measurement overlays a first level of spatial variability at different scales.

Table 2.1 Potential agricultural applications for resistivity (ER), electromagnetic induction (EM), and ground-penetrating radar methods (GPR) **(**modified from Allred et al., 2008)

Application	**ER**	**EM**	**GPR**	**Literature source**
Determining clay-pan depth	×	×		e.g., Doolittle et al., (1994)
Soil water content determination	×	×	×	e.g., Garrè et al., (2013); Grote at al., (2003); Huang et al., (2016); Lunt et al., (2005); Sheets and Hendrickx, (1995)
Soil salinity assessment	×	×		Doolittle et al., (2001); Hendrickx et al., (1992); Rhoades and Ingvalson, (1971); Shea and Luthin, (1961)

For an agriculture prospective, geophysical applications have been explored mainly in relation to soil moisture and salinity detection, as well as the structural status of surface soil layers (Samouëlian et al., 2005).

Agricultural geophysics measurements can be applied at a wide range of scales and often exhibit significant variability both temporally and spatially (Allred et al., 2008). Agricultural geophysics investigations are commonly (although certainly not always) focused on delineating small- and/or large-scale objects/features within the soil profile also over very large areas.

Agricultural geophysics tends to be heavily focused on a two meters zone directly beneath the ground surface, which includes the crop root zone and all, or at least most, of the soil profile. With regard to the application of geophysics to agriculture, this extremely shallow depth of interest is certainly an advantage, in one sense because most geophysical methods have investigation depth capabilities that far exceed two meters (Allred et al., 2008). The ability to image and quantify soil-moisture changes at important spatial and temporal scales with minimal disturbance to the environment and the possibility to acquire data in difficult terrain are two additional advantages.

The development of geophysical methods (Allred et al., 2008; Vereecken et al., 2006; Binley et al., 2015) provides potentially effective approaches to the challenges above (e.g. Bitella et al., 2015), especially when the study of soil–root plant interactions plays a fundamental role. In particular, the specificity of plant root distribution dynamics (e.g., due to

growth, phenological stage, water and nitrogen availability) and soil texture variability, combined with the pulsed nature of water inputs, create highly heterogeneous situations, in terms of root water uptake (RWU) patterns. These patterns can be difficult to capture even with dense networks of point sensors (Jayawickreme et al., 2014) (e.g., dielectric based). In this respect, there is a growing demand of near-surface observing technologies for studying a wide spectrum of phenomena in the soil, which may have implications also in the agricultural context (Bitella et al., 2015).

Recent studies (Cassiani et al., 2015; Consoli et al., 2016 b; Satriani et al., 2015) have demonstrated that geophysical techniques can support the irrigation operations in terms of both water amounts and irrigation timing. In this context, geophysical imaging techniques are being recognised as very attractive tools for the identification of water dynamics in the vadose zones (e.g. Binley et al., 2002; Deiana et al., 2007, 2008; Cassiani et al., 2012, 2015, 2016).

2.1.1. Electrical resistivity tomography

Electrical resistivity tomography (ERT – see Binley and Kemna, 2005) is an active source geophysical method that uses a low-frequency electrical current, galvanically injected into the ground between two electrodes (current source electrodes), and measures the potential between two or more different electrodes (potential electrodes). This pattern is repeated through many combinations of transmitting and receiving electrodes along a line or grid (or with borehole electrodes), and the result is a cross section or a volume distribution of electrically resistive or conductive regions in

the subsurface. The current, voltage, electrode spacing, and electrode configuration are used to calculate the apparent resistivity (i.e., the inverse of electrical conductivity).

As reported above, ERT in general is a technique suitable for the investigation of ground properties, based on the response of soil materials to the flux of electrical charges.

ERT prospecting has recently improved with respect to measurement time. The improvement of computer-controlled multi-channel resistivity-meters using multi-electrode arrays has led to an important development of electrical imaging. Switching units allow any combination of four electrodes to be connected to the resistivity-meter at any time. The electrical data measurement is then fully automated and acquisition can be rapid (Binley et al., 1996).

2.1.1.1 Measurement errors

Assess the data quality is the first step in the direct current (DC) resistivity data processing.

Binley et al (2015b) underline that DC resistivity data can suffer from a range of sources of error, which, if not addressed correctly can have a significant impact on the interpretation of survey results. Binley et al (2015b) report useful recommendation to control measurement errors. Firstly, high contact resistance between the measurement electrodes and the ground can be particularly problematic especially in dry soil. Secondly, it is important to take into account the receiver voltage levels in a given measurement: high geometric factors, combined with low input voltage can

lead to voltages that are close to instrument resolution. Thirdly, natural self-potentials also need to be accounted for particularly if they are not stable over time.

Finally, negative apparent resistivity values in DC resistivity surveys often highlight problems with contact resistance and signal strength. Such measurements may be assessed to be erroneous, however, through appropriate modeling, these measurements provide information about the subsurface and should not be rejected on the grounds of polarity alone.

The quality of DC resistivity measurements is often determined through repeatability, i.e. by assessing the variability of responses from multiple injected cycles. Whilst these are useful direct in-field indicators of data quality, sources of error may not be random and could, in theory, repeat. An alternative measure of data quality is reciprocity (e.g. Parasnis, 1988). Measurements made after switching injection and receiver pairs should be identical; the difference is often termed a reciprocal error and can often be a much better assessment of data quality in DC resistivity surveys (see, Slater and Binley, 2006).

2.1.1.2 Modelling and inversion

Whereas the forward model (F_m) computes the apparent resistivity from a spatial distribution of resistivity, the inverse model derives the set of spatial geoelectrical properties that is consistent with the observed data (apparent resistivity) (Binley et al., 2015b).

The goal is to derive the distribution of the electrical properties (resistivity model) that satisfy the transfer resistance observations for a given set of measurements (resistance data, i.e., the ratio between potential and current), within a specified tolerance level and appropriate model constraints.

Unconstrained inverse modelling of geoelectrical data is inherently non-unique (often underdetermined, too many unknowns and too few equations), in that there are likely to exist a large number of geoelectrical models (e.g. distributions of resistivity) that comply with the observed data. The solution varies, depending on how the problem is posed. Furthermore, without appropriate constraints, errors (e.g. numerical rounding errors) can propagate and lead to an unstable solution.

As reported in Binley et al., (2015b) most geoelectrical inverse models used today are based on a least squares fit between data and model parameters. The data-model misfit is expressed as:

$$\Psi_d == \left(d - F(m)\right)^T W_d^T W_d \left(d - F(m)\right) \qquad (2.1)$$

where Ψ_d is the objective function; d are the data (e.g. measured apparent resistivities); $F(m)$ is the set of equivalent forward model estimates with parameter set m; W_d is a data weight matrix, which, if we consider the uncorrelated measurement error case and ignore forward model errors, is a diagonal matrix with entries equal to the standard deviation

of each measurement, quantified using the reciprocal error (Slater et al., 2000).

Attempts have been made to minimize Ψ_d in Eq. (2.1). Binley et al., (2015b) report that the Occam's method proposed by Constable et al.(1987) offered a major breakthrough in geoelectrical inverse modelling and is fundamental to the majority of inverse solutions of DC resistivity today. The method of Constable et al. (1987) searches for the smoothest model (set of parameters) that is consistent with the data. The label "Occam's" was used by Constable et al. (1987) to emphasize the search for the simplest model (after Occam's razor). Their approach utilizes spatial regularization (Tikhonov and Arsenin, 1977) to enforce smoothing, which also helps ensure a stable and unique solution. Regularizing the minimization problem can be achieved by adding a model penalty term:

$$\Psi_m == m^T R m \tag{2.2}$$

where R is a roughness matrix that describes a spatial connectedness of the parameter call values. Then, the function to be minimized is:

$$\Psi_{tot} == \Psi_d + \alpha \Psi_m \tag{2.3}$$

where α is is a regularization parameter which optimizes the trade-off between the minimized data misfit and the minimized model (i.e., controls the emphasis of smoothing).

In an Occam's solution we seek to satisfy the minimization of equation 2.3, subject to the largest value of α. The process

is achieved by utilizing the Gauss Newton approach, which results in the iterative solution of:

$$(J^T W_d^T \Psi_d J + \alpha R)\Delta m == J^T W_d^T \left(d - F(m_k)\right) + \alpha R m_k \quad (2.4)$$

$$m_{k+1} = m_k + \Delta m$$

where J is the Jacobian (or sensitivity) matrix, given by $J_{i,j}=\delta d_i/\delta m_i$; m_k is the parameter set at iteration k; Δm is the parameter update at iteration. For the DC resistivity case, the inverse problem is typically parameterized using log-transformed resistivity.

The conventional regularization approach in ERT provides an additional constraint to make the problem less underdetermined by favouring models with minimum structure over rougher models that might fit the data equally well (de Groot-Hedlin and Constable, 1990).

2.1.1.3 Time-lapse inversion

Individual images corresponding to different times can be combined and inverted as ratio or differences. If we have two datasets, d_t and d_0 then we can compute a combined (ratio) dataset from:

$$d_r = \frac{d_t}{d_0} F(\sigma_{\text{hom}}) \quad (2.5)$$

where d_r is the resistance ratio, d_t e d_0 are the dataset collected at the time (t) and at the initial condition (0), and $F(\sigma_{ohm})$ is resistance value obtained by running the forward model for an arbitrarily chosen conductivity (100 Ohm m). The inverted

image will then show any changes relative to this reference value.

2.1.2. ERT: application in agricultural contexts

Among the geophysical applications in agriculture and more generally for environmental purposes, electrical resistivity tomography (ERT) is considered one of the most effective methods, as it offers high spatial (and temporal) resolution, combined with a non-invasive character causing no disturbance during soil monitoring (Michot et al. 2003; al Hagrey 2007).

ERT is a minimally invasive technique that obtains information on the variability of the electrical resistivity of the subsoil which, when related to water and solute content, can help to spatialize water and nutrient uptake active zones (e.g. Srayeddin and Doussan, 2009).

Several authors have successfully used ERT to observe transient state phenomena in the soil-plant (SP) *continuum*. In particular, ERT and other electrical techniques have been adopted to monitor RWU processes of herbaceous crops both in the laboratory (Werban et al., 2008) and at field scale (e.g., Srayeddin and Doussan, 2009; Garré et al., 2011; Beff et al., 2013; Cassiani et al., 2015; Shanahan et al., 2015; Consoli et al., 2016 a and b). These results have demonstrated the match between the temporal soil water content (SWC; m^3 m^{-3}) changes and the electrical resistivity patterns.

Using the 2-D time-lapse ERT monitoring, Michot et al. (2003) identified the soil drying patterns in the shallow soil

where roots activity is more intense. Other authors applied ERT to eco-physiological studies involving fruit crops such as orange (Cassiani et al., 2015; Moreno et al., 2015), apple (Boaga et al., 2013), olive and poplar trees (al Hagrey, 2007) as well as natural forest (Nijland et al., 2010; Robinson et al., 2012).

Brillante et al. (2015), however, noted that the use of ERT in eco-physiological studies, coupled with parallel monitoring of plant water status, is still rare and therefore needs further investigation in order to answer to new questions on plant and soil relationships, and open the way to new techniques for water management in agricultural scenarios.

The studies highlighted above, show the potential of ERT for these applications, even if difficulties in the interpretation of the measured electrical resistivity patterns remain a frequent limitation especially under field conditions. First, electrical resistivity is a function of a number of soil properties, including the nature of the solid constituents (particle size distribution, mineralogy), the arrangement of voids (porosity, pore size distribution, connectivity), the degree of water saturation (water content), the pore electrical conductivity (solute concentration) and temperature. The variability of these factors needs to be restricted (e.g., adopting time-lapse measurements) or measured independently and a fitting calibration equation needs to be established (e.g., Michot et al., 2003). Second, rapid changes in the soil-plant-atmosphere *continuum*, such as an infiltration front passing after irrigation inputs and/or a heavy rain, require high temporal resolution of the measurement to avoid temporal aliasing (e.g., Koestel et al., 2009). Finally, RWU processes are highly

spatially variable and require at least a decimetric spatial resolution (Michot et al., 2003).

2.2. Overview of evapotranspiration and sap-flow fluxes measurements

2.2.1 Micro-meteorological methods

Evapotranspiration (ET) is the term used to describe the part of the water cycle which removes liquid water from an area with vegetation and into the atmosphere by the processes of both transpiration and evaporation (Allen et al., 1998).

From an energetic point of view, Rana and Katerji (2000) described ET as the energy employed for transporting water from the leaves and plant organs to the atmosphere as vapour. The amount of energy, that is at the base of the ET process, is the latent heat (λE, with λ latent heat of vaporization equal to 2.45×10^6 J kg^{-1} at 20 °C) and is expressed as energy flux density (W m^{-2}).

Under this form, ET can be measured with the so-called micrometeorological methods. These techniques are physically-based and depend on the laws of thermodynamics and on the transport of scalars into the atmosphere above the canopy. Katerji and Rana (2008) report that micrometeorological applications need accurate measurements of meteorological variables on a short temporal scale with suitable sensors placed above the canopy. Due to the conservative hypothesis of all the flux densities above the crop, the micrometeorological methods can be

applied only on large flat surfaces with uniform vegetation. Micrometeorological methods for measuring or estimating ET are generally referred to plot scale.

2.2.1.1. Eddy covariance technique

The transport of scalar (vapour, heat, carbon dioxide) and vectorial quantities (i.e., momentum) in the low atmosphere in contact with the canopies is mainly driven by air turbulence (Rana and Katerji, 2000; Katerji and Rana , 2008).

The eddy covariance (EC) method is a direct measurement of a turbulent flux density of a scalar across horizontal wind streamlines (Paw U et al., 2000).The calculation of turbulent fluxes is based on the Navier-Stokes equation and similar equations for temperature or gases by the use of the Reynolds' postulates. For details on the theory, see Stull (1988). The equations for determination of surface fluxes are obtained by further simplifications, these are:

- stationarity of the measuring process;
- horizontal homogeneity of the measuring field;
- validity of the mass conservation equation;
- negligible density flux;
- statistical assumptions, for example statistical independence and the definition of the averaging procedure;
- the Reynolds' postulates and the postulate which is used for the calculation of the eddy covariance method should be valid;

– the momentum flux in the surface layer as well as the temperature flux (analogue equations for water vapour and gaseous fluxes) doesn't change with the height within about 10% to 20% of the flux (Foken and Wichura, 1996).

When certain assumptions are valid, theory predicts that energy fluxes from the surface can be measured correlating to the vertical wind fluctuations from the mean (w') in concentration of the transported admixture (Rana and Katerji, 2000). A direct method for measuring λE, above a vegetative surface over a homogeneous canopy, is to measure simultaneously vertical turbulent velocity and specific humidity fluctuations and to determine their covariance over a suitable sampling time. So that, for latent heat flux (λE) we can write the following covariance of vertical wind speed and vapour density:

$$\lambda E = \lambda \overline{w' q'} \qquad (2.6)$$

with w' is the vertical wind speed (m s^{-1}) and q' is the air humidity (kg m^{-3}).

In this way, measurements of the instantaneous fluctuations of w' and q', at a frequency sufficient for obtaining the contribution from all the significant sizes of eddy, permit to calculate ET by summing their product over a hourly time scale. To measure ET with this method, vertical wind fluctuations must be measured and acquired at the same time as the vapour density. The first one can be measured by a

sonic anemometer, the second one by a fast response hygrometer (Katerji and Rana, 2008).

The sensible heat (H) using the EC technique by analogy with the expression above (Eq. 2.6), can be written as

$$H = \rho_{air} c_p \overline{w'T'} \qquad (2.7)$$

with ρ_{air} the air density and c_p the specific heat of air at a constant pressure.

The wind speed (w') and temperature fluctuations (T') are measured by means of sonic anemometer and fast response thermometer, respectively (Katerji and Rana, 2008).

Sensors must measure vertical velocity, temperature and humidity with sufficient frequency response to record the most rapid fluctuations important to the diffusion process. Typically, a frequency of the order of 5-10 Hz is used, but the response-time requirement depends on wind speed, atmospheric stability and the height of the instrumentation above the surface. Outputs are sampled at a sufficient rate to obtain a statistically stable value for the covariance (Drexler et al., 2004). If a 30-minute sampling time is used over the whole day, then remarkable errors will be reduced (Foken, 2008). Wind speed and humidity sensors should be installed close to each other but sufficiently separated to avoid interference. When the separation is too large, underestimation of the flux may result. Some disadvantages of EC method include sensitivity to fetch and high cost and maintenance requirements (Brotzge and Crawford, 2003;

Foken, 2008). High-frequency wind vector data are usually obtained with a three-dimensional sonic anemometer. These instruments provide the velocity vector in all three directions and, therefore, corrections can be applied for any tilt in the sensor and mean streamline flow. A wide range of humidity sensors have been used in EC systems including thermocouple psychrometers, Lyman-alpha and krypton hygrometers, laser-based systems and other infrared gas analysers (Drexler et al., 2004). Since the size of the turbulence eddies increases with distance above the ground surface, both the measuring path length and the separation between a sonic anemometer and an additional device depend on the height of measurement. Therefore, to reduce the corrections of the whole system the measurement height must be estimated on the basis of both the path length of the sonic anemometer and the separation of the measuring devices. In addition, the measuring height should be twice the canopy height in order to exclude effects of the roughness sublayer (Foken, 2008).

The EC technique is the most direct method for quantifying the turbulent exchange of energy and trace gases between the Earth's surface and the atmosphere (Mauder et al., 2010). However, the derivation of the mathematical algorithm is based on a number of simplifications so that the method can be applied only if these assumptions are exactly fulfilled. The quality of the measurements depends mainly on the application conditions and accurate use of the corrections than on the available highly sophisticated measuring systems. Therefore, experimental experience and knowledge of the special atmospheric turbulence characteristics have a high

relevance. The most limiting conditions are horizontally homogeneous surfaces and steady-state conditions (Foken, 2008a). These requirements are often violated in complex terrain, and their non-fulfilment reduces the quality of the measurement results. Foken and Wichura (1996) address this problem by assigning quality flags to the fluxes in accordance with the deviations found between parameterisations under ideal conditions and those actually measured. Secondly, in a heterogeneous environment the land use types contributing to the measurements change with the source area of the fluxes. This source area, which can be calculated by footprint models, defines the region upwind of the measurement point, which influences the sensor's measurements and is dependent on measurement height, terrain roughness, and boundary layer characteristics, such as the atmospheric stability. As most sites in monitoring networks are set up to measure fluxes over a specific type of vegetation, the changing contribution of this type of land use, under different meteorological conditions, has to be considered in order to assess how representative the measurements are (Göckede et al., 2004). The latter can lead to a bias of the flux estimate that becomes apparent in a lack of energy balance closure, usually ranging between 10 and 30% of the available energy at the surface. It is possible to minimize the deviation between actual and measured EC fluxes through an optimal equipment configuration and through application of adequate correction methods. The typical processing steps are:

– tilt correction,
– buoyancy correction (also Schotanus correction),

- density correction (also WPL correction, see Webb et al. 1980),
- damping (attenuation) correction (Spank and Bernhofer, 2008).

The application of correction methods is closely connected with the data control. The data control starts with the exclusion of missing values and outliers. A basic condition for applying the EC method is the assumption of a negligible mean vertical wind component; otherwise, advective fluxes must be corrected. This correction is called tilt correction and includes the rotation of a horizontal axis into the mean wind direction. The first correction is the rotation of the coordinate system around the z-axis into the mean wind. The second rotation is around the new y-axis until the mean vertical wind disappears. With these rotations, the coordinate system of the sonic anemometer is moved into the streamlines (Foken, 2008). An important correction to the actual available turbulence spectra is the adjustment of the spectral resolution of the measuring system. Hence, the resolution in time (time constant), the measuring path length, and the separation between different measuring paths must be corrected. The spectral correction is made using transfer functions (Foken, 2008). WPL-correction is a density correction, caused by ignoring density fluctuations, a finite humidity flux at the surface, and the measurement of gas concentration per volume unit instead of per mass unit. WPL-correction is large if the turbulent fluctuations are small relative to the mean concentration. The conversion from volume into mass-related values using WPL-correction is not applicable if the water vapour concentrations or the concentrations of other gases are

transferred into mol per mol dry air before the calculation of EC. However, the calculation is possible depending on the sensor type and if it is offered by the manufacturers (Foken, 2008). Hence, the quality assurance of turbulence measurements with EC method is a combination of the complete application of all corrections and the exclusion of meteorological influences such as internal boundary layers, gravity waves, and intermitted turbulence. Quality tests are used to validate the theoretical assumptions of the method such as steady-state conditions, homogeneous surfaces, developed turbulence (Foken, 2008).

2.2.2 Sap flow by heat pulse technique

This method measures the water loss at the plant scale. Sap flow is closely linked to plant transpiration (T_{SF}) by means of simple accurate models (Katerji and Rana, 2008). Sap flow methods are easily automated, so continuous records of plant water use with high time resolution can be obtained. Moreover, these methods can be used anywhere with minimally disturbance at the site. However, when sap flow measurements are adopted to estimate T_{SF} for stands of vegetation, appropriate methods of scaling from plant to unit area of land must be used (Smith and Allen, 1996).

Different methods are used to measure sap flow in plant stems or trunks. The most common are: heat pulse velocity (HPV) methods; heat balance method; thermal dissipation probe method or Granier method. In HPV methods, sap flow is estimated by measuring HPV, stem area and xylem conductive area (Katerji and Rana, 2008), using a linear heater and temperature probes inserted radially into the plant

stem or trunk (Green et al., 2003a) and parallel to each other (Cohen et al., 1981). Thermocouples or thermistors are positioned along the length of the temperature probe to monitor temperature rise at various radial positions within the stem. At each position, the HPV is determined by measuring the time between the introduction of the heat pulse and the occurrence of the maximum temperature rise. HPVs are converted into the sap flux densities and then integrated over the cross-sectional area of the stem or trunk to yield the volumetric sap flow rate (Kluitenberg and Ham, 2004). These methods include the heat pulse velocity (HPV) method and the T-max method.

HPV method is based on the compensation heat pulse method. Swanson (1962) was one of the first to utilize Marshall's analytical solutions to heat flow equation (Marshall, 1958), by applying them the analysis of the 'compensation' heat pulse method in which two temperature probes are placed asymmetrically in either side of a line heater source that is inserted radially into the tree stem.

Figure 2.1 shows the configuration of a single set of heat-pulse probes implanted radially into a stem of radius *r* at the cambium and *h* at the heartwood boundary. In Figure 2.1, the upstream temperature sensor is installed at a distance below the heater (X_u) and the downstream sensor at a distance above the heater (X_d), (Smith and Allen, 1996). The heater introduces a brief pulse of heat (1-2 s) into the stem and a data logger measures the time delay (t_z) for an equal temperature rise at both sensors (Green, 2009).

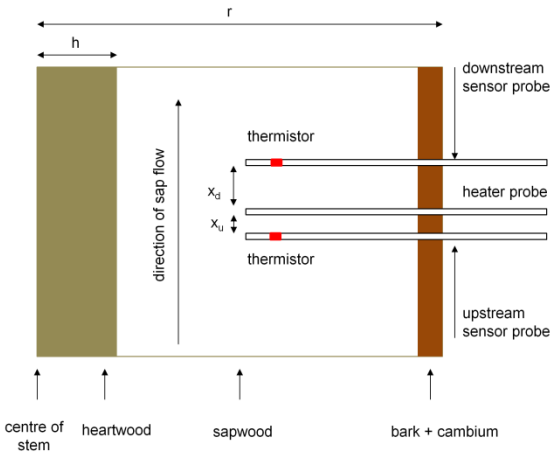

Figure 2.1 Configuration of a single set of heat-pulse probes implanted radially into a stem (modified from Smith & Allen, 1996)

Swanson (1962) showed that if the temperature rise following the release of a pulse of heat is measured at distances X_u (m) upstream and X_d (m) downstream from the heater, then the HPV can be calculated as:

$$V_z = \left(\frac{X_d + X_u}{2t_z} \right) \tag{2.8}$$

where t_z (s) is the time delay for the temperatures at points X_d and X_u to become equal.

Equation 2.8 implies that, following the application of an instantaneous heat-pulse, the centre of the heat-pulse is

convected downstream, from the heater, to reach the midway point between the two temperature sensor after t_z. Equation 2.8 is particularly suited to data logging since it only requires electronics to detect a null temperature difference and an accurate timer to measure t_z. The t_z (s) are the only data to be recorded, since the distances X_u and X_d remain constant. This estimate of V_z (m s^{-1}) is the 'raw' HPV. The calculation of V_z from Eq. 2.8 is based on Marshall's (1958) idealized theory and assumes that heat-pulse probes have no effect on the measured heat flow. Actually, convection of the heat-pulse is disturbed by the presence of the heater and temperature probes, and by the disruption of xylem tissue associated with their placement. These disturbances produce a systematic underestimation of the measured HPV (Cohen et al., 1981). Consequently, the HPV must be corrected for the probe-induced effects of wounding. This correction can be applied empirically, or it can be based on sound physical principals, using an equation of the form:

$$V_c = a + bV_z + cV_z^2 \qquad (2.9)$$

where V_c (m s^{-1}) is the corrected HPV and V_z is the raw HPV given by Eq. 2.8. The correction coefficients a, b, and c have been derived by Swanson and Whitfield (1981) from numerical solutions of Marshall's (1958) equations, for various wound sizes. Once V_c has been determined, the next step is to relate it to the actual sap flow. Marshall's (1958) analysis showed that if the sap and woody matrix are considered to form a homogeneous medium, then the sap flux density, j (m s^{-1}), can be calculated from:

$$j = (kF_M + F_L)V_c \quad (2.10)$$

where F_M and F_L are the volume fractions of wood and water, respectively; k is a coefficient related to the thermal properties of the woody matrix (Becker and Edwards, 1999), and it is assumed to be constant within and between species (Green et al., 2003b; Green, 2009).

Volume fractions F_M and F_L expressed in Eq. 2.10 are determined from the Archimede's principle, as in the following:

– a core sample is taken and its fresh weight, M_F (kg), is determined. This weight is equal to the mass of water and the mass of dry wood, since the mass of air is negligible;

– the core sample is then submerged in a beaker of water where a mass balance is determined. The balance reading will indicate an immediate increase in mass, which equals the displacement of water, D_T (kg). The total volume, V_T (m^3), of the sample is then equal to ρ_L times D_T, where the density of water, ρ_L, is assumed to be 1000 kg m^{-3};

– the core sample is then oven-dried to determine the mass of dry wood, M_D (kg). The difference between the fresh weight and the dry weight, (M_F-M_D) is equal to the mass of water, M_L (kg), in the fresh core sample.

Thus, the volume fraction of water is calculated as follows:

$$F_L = M_L/(\rho_L V_T) \quad (2.11)$$

Similarly, the volume fraction of wood is equal to:

$$F_M = M_D/(\rho_M V_T) \quad (2.12)$$

where the density of dry wood (ρ_M) is 1530 kg m^{-3}.

Equation 2.10 provides an estimate of j at any point in the conducting sapwood. It is widely recognized that sap flux density is not uniform throughout the sapwood, but rather peaks at a depth of 10-20 mm from the cambium. Consequently, sampling at several depths in the sapwood is necessary to characterize the profile of sap flow velocity.

A volumetric measure of total sap flux can be obtained by integrating these point estimates over the sapwood conducting area (Green, 2009).

As described in this Chapter, the state-of-the-art about SPAC monitoring includes numerous stand-alone methodologies. The aim of this PhD work is the assimilation of geophysical methods with other more conventional (ET and sap-flow fluxes measurements) in order to help solving the complexity of the SPAC interactions.

Chapter 3

Case study 1

Case study 1

This Chapter describes an experimental application (Case study 1) corresponding to the joint use of electrical resistivity tomography (ERT), sap flow (HPV) and eddy covariance (EC) data to characterize the unsaturated soil volume of an orange tree root-zone in semi-arid environment.

My support in this study was mainly related to the geoelectrical measurements at the field scale and in laboratory. With reference to the latter, I carried out lab-analyses at the Department of Geoscience (Padua University) in order to calibrate the resistivity-soil moisture relationship on soil samples collected at Case study 1.

The specific goals of this study were:

- to study the feasibility of a small-scale monitoring of root zone processes using time-lapse 3-D ERT;
- to assess the value of the data for a quantitative description of hydrological processes at the tens of centimeter scale;
- to interpret these data with the aid of a physical hydrological model, in order to also derive information on the root zone physical structure and its dynamics.

The overall results of this Chapter have been published in Hydrology and Earth System Sciences, 19(5), 2213–2225 by Cassiani, G., Boaga, J., Vanella, D., Perri, M. T., & Consoli, S. (2015).

3.1 Field site description

The experimental site was an orange orchard, planted with about 20 year-old trees (*Citrus sinensis*, cv Tarocco Ippolito) (Figure 3.1). The field was located in Lentini (Eastern Sicily, Lat. 37°16' 57.80" N, Long. 14°53' 22.35" E) in a Mediterranean semi-arid environment, characterized by an annual average precipitation of around 550 mm, very dry summers and average air temperature of 7°C in winter and 28°C in summer. The site presented conditions of crop homogeneity, flat slope, dominant wind speed direction for footprint analysis and quite large fetch that were ideal for EC micrometeorological measurements. The planting layout was 4.0 m × 5.5 m and the trees were drip irrigated with 4 in-line drippers per plant, spaced about 1 m, with 16 L h^{-1} of total discharge (4 L h^{-1} per dripper). Trees were well watered by irrigation supplied every day from May to October, with irrigation timing of 5 h d^{-1}. The study area had a mean leaf area index (LAI) of about 4 m^2 m^{-2}, measured by a LAI-2000 digital analyser (LI-COR, Lincoln, Nebraska, USA). The mean PAR (photosynthetic active radiation) light interception was 80% within rows and 50% between rows; the canopy height (h_c) was 3.7 m.

The soil characterization was performed via textural and hydraulic laboratory analyses, according to the USDA standards, and it is classified as loamy sand. In this study, we used van Genuchten's (1980) analytical expression to describe soil water retention and a falling-head permeameter to determine the hydraulic conductivity at saturation. For each soil sample, the moisture content at standard water

potential values was determined by a sandbox and a pressure membrane apparatus (Aiello et al., 2014).

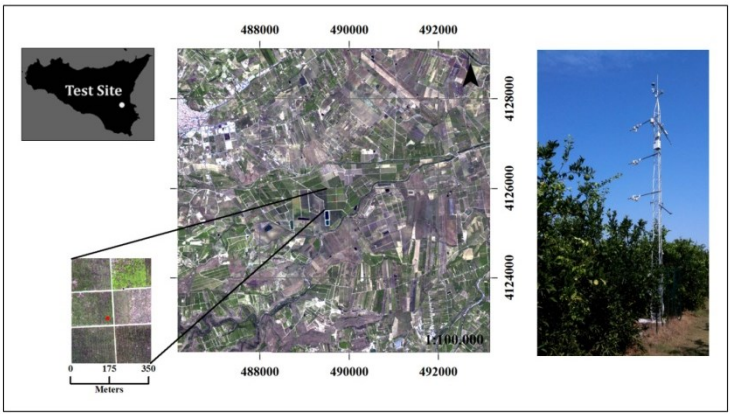

Figure 3.1 Location of Case study 1 in Sicily (Italy)

Three soil moisture profiles were measured in the field using time-domine reflectometry (TDR) probes. Calibrated Campbell Scientific CS616 water content reflectomers (±2.5% of accuracy) were installed to monitor every hour the changes of volumetric soil water content (θ). The TDR probe installation was designed to measure soil water content variations with time in the soil volume afferent to each plant. For each location, the TDR equipment consisted of two sensors inserted vertically at 0.25 m and 0.40 m depth and of two sensors inserted horizontally at 0.25 m depth with 0.20 m in between. The data that are discussed here (see results section 3.5.3) correspond to the TDR probes located at about 1.5 m from the orange tree we monitored with ERT.

Hourly meteorological data (incoming short-wave solar radiation, air temperature, air humidity, wind speed and rainfall) were acquired by an automatic weather station located about 7 km from the orchard and managed by SIAS (Agro-meteorological Service of the Sicilian Region). For the dominant wind directions, the fetch was larger than 550 m. For the other sectors, the minimum fetch was 400 m (SE).

3.2 Small scale 3D-ERT monitoring

ERT (e.g. Binley and Kemna, 2005) was used as key technique to monitor the soil moisture content distribution in the soil volume surrounding the orange tree.

3.2.1 Small scale 3D-ERT setup

The three-dimensional ERT system consisted of 48 buried electrodes, placed on 4-instrumented micro-boreholes, with 12 electrodes each. Electrodes were made of a metal plate wound around a one inch plastic pipe, and are spaced 0.1 m along the, thus the shallowest and the deepest are respectively at 0.1 m and 1.2 m below the surface. The boreholes were placed at the vertices of a square, having a side of 1.3 m, that has the orange tree at its centre. The system was completed by 24 electrodes at the ground surface, placed along a square grid of about 0.21 m side, covering the 1.3 m x 1.3 m square at the surface (Figure 3.2). This setup allowed a homogeneous coverage of the surface of the control volume. A similar 3D ERT setup was tested in an apple orchard by Boaga et al., (2013). The chosen acquisition scheme was a skip-zero dipole-dipole configuration, i.e. a configuration where the current dipoles and potential dipoles are both of

minimal size, i.e. they consist of neighbouring electrodes e.g. along the boreholes. This setup ensures maximal spatial resolution (as good as the electrode spacing, at least close to electrodes themselves) provided that the signal/noise ratio was sufficiently high.

Table 3.1 Times of acquisitions and irrigation schedule

Acquisition #	Starting time (LT)	Ending time (LT)	Irrigation schedule	Date
0 (background)	10:40	11:00	11:30 to 16:30 4 l/h from each dripper	October 2, 2013
1	12:00	12:20		
2	13:00	13:20		
3	14:15	14:35		
4	15:00	15:20		
5	16:00	16:20		
6	17:00	17:20		
7	10:15	10:35	7:00 to 12:00 4 l/h from each dripper	October 3, 2013
8	11:05	11:25		
9	12:00	12:20		
10	13:00	13:20		
11	14:00	14:20		
12	15:00	15:20		
13	15:45	16:05		

We conducted ERT measurements repeated using the above apparatus for about two days, starting on October 2, 2013 at 11:00 am, and ending the next day at about 16:00. The schedule of the acquisitions and the irrigation times (local time, LT) is reported in Table 3.1. Note that the background ERT survey was acquired on October 2 at 11:00 before the first irrigation period was started, so that all changes caused by irrigation and subsequent evapotranspiration (ET) can be

referred to that instant (initial conditions). Note that prior to October 2, 2013, irrigation had been suspended for at least 15 days. Note also that only one dripper – with a flow of about 4 l h^{-1} – was located at the surface of the control volume defined by the ERT setup.

3.2.2 Small scale 3D-ERT data processing

The data quality was assessed using a full acquisition of reciprocals to estimate the data error level (see e.g., Binley et al., 1995; Monego et al., 2010).

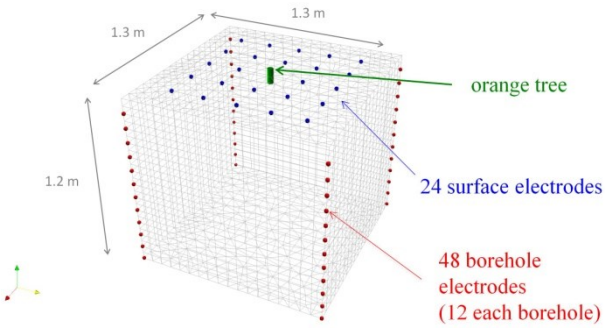

Figure 3.2 Electrode geometry around the orange tree and 3-D mesh used for ERT inversion

Consistently, we used for the 3D data inversion an Occam approach as implemented in the R3 software package (Binley, 2014) accounting for the error level estimated from the data themselves. The relevant three-dimensional computational mesh is shown in Figure 3.2. At each time step, about 90-95 % of the dipoles survived the 10%

reciprocal error threshold. In order to build a time-consistent data set, only the dipoles surviving this error analysis for all time steps were subsequently used, reducing the number to slightly over 90% of the total. The absolute inversions were run using the same 10% error level. Time-lapse inversions were run at a lower error level equal to 2 % (consistently with the literature – e.g., Cassiani et al., 2006).

3.3 Micro-meteorological measurements

Measured energy fluxes, by EC system mounted on a micrometeorological fluxes tower, were used to calibrate like an input the hydrologic model of the root-zone area (see paragraph 3.5.3). Continuous energy balance measurements have measured since 2009 at the Case study 1 site. Equipment mounted on the EC micrometeorological tower at Case study 1, herein described, is reported in Figure 3.3.

Net radiation (R_n, W m^{-2}) was measured with two CNR 1 Kipp&Zonen (Campbell Scientific Ltd) net radiometers at a height of 8 m.

Soil heat flux density (G, W m^{-2}) was measured with three soil heat flux plates (HFP01, Campbell Scientific Ltd) placed horizontally 0.05 m below the soil surface. Three different measurements of G were selected: in the trunk row (shaded area), at 1/3 of the distance to the adjacent row, and at 2/3 of the distance to the adjacent row. G was measured as the mean output of three soil heat flux plates. Data from the soil heat flux plates was corrected for heat storage in the soil above the plates.

Air temperature and three wind speed components were measured at two heights, 4 and 8 m, using fine wire thermocouples (76 μm diameter) and sonic anemometers (Windmaster Pro, Gill Instruments Ltd, at 4m, and a CSAT, Campbell Sci., at 8 m). A gas analyzer (Li-7500, Campbell Sci.) operating at 10 Hz was installed at 8 m. The raw data were recorded at a frequency of 10 Hz using two synchronized data loggers (CR3000, Campbell Sci.).

The EC measurement system and the data processing followed the guidelines of the standard EUROFLUX rules (Aubinet et al., 2000). A data quality check was applied during the post processing together with some routines to remove the common errors: running means for de-trending, three angle coordinate rotations and de-spiking. Stationarity and surface energy closure were also checked (Kaimal and Finningan, 1994).

The freely distributed TK2 package (Mauder and Foken, 2004) was used to determine the first and second order statistical moments and latent (LE) and sensible (H) heat fluxes on a half-hourly basis following the protocol used as a comparison reference described in Mauder et al., (2007).

Low frequency measurements were taken for air temperature and humidity (HMP45C, Vaisala), wind speed and direction (05103 RM Young), and atmospheric pressure (CS106, Campbell Scientific Ltd) at 4, 8 and 10 m.

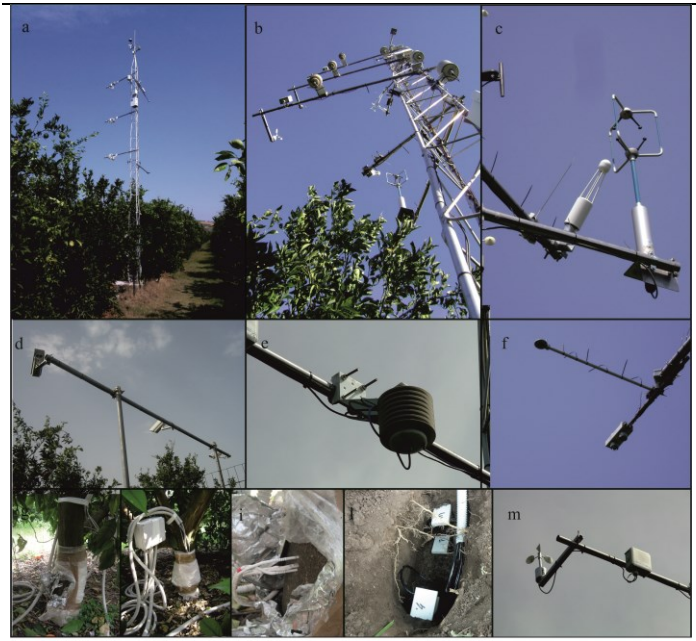

Figure 3.3 EC micrometeorological equipment at Case study 1. EC tower (a, b); 3D sonic anemometer, gas analyzer and fine wire thermocouples (c); infra-red remote temperature sensor (d); temperature and relative humidity probe (e); net radiometer (f); sap flow sensors (g, h, i); TDR probes (l); anemometer (m)

3.4 Transpiration measurements at tree level

Measurements of water consumption at tree level were taken using the heat pulse velocity (HPV) technique that is based on the measurement of temperature variations (ΔT), produced by a heat pulse of short duration (1-2 s), in two temperature probes installed asymmetrically on either side of a linear heater that is inserted into the trunk.

For HPV measurements, two 4 cm sap flow probe with 4 thermocouples embedded (Tranzflo NZ Ltd., Palmerston North, NZ) were inserted in the trunks of the trees, belonging to the area of footprint of the micro-meteorological EC tower. The probes were positioned at the North and South sides of the trunk at 0.5 m from the ground and wired to a data-logger (CR1000, Campbell Sci., USA) for heat-pulse control and measurement. The sampling interval was 30 min. The temperature measurements were obtained by means of ultra-thin thermocouples that, once the probes are in place, are located at 5, 15, 25 and 45 mm within the trunk. Data were processed according to Green et al., (2003b) to integrate sap flow velocity over sapwood area and calculate transpiration. In particular, the volume of sap flow in the tree stem was estimated by multiplying the sap flow velocity by the cross sectional area of the conducting tissue. To this purpose, fractions of wood ($F_M = 0.48$) and water ($F_L = 0.33$) in the sapwood were determined on the trees where sap flow probes were installed. Wound-effect correction (Green et al., 2003a) were done on a per-tree basis.

3.5. Results and discussion

3.5.1 Evapotranspiration and transpiration fluxes

Surface energy balance measurements at Case study 1 site, during the irrigation season in 2013, showed that the sum of sensible (H) and latent (LE) heat flux was highly correlated (r^2>0.90) (Figure 3.4) to the sum of net radiation (R_N) and soil heat flux (G) (Castellvì et al., 2012; Consoli and Papa, 2013).

A linear fit between the two quantities showed a certain energy balance un-closure. The percentage of un-closure (about 10%) was in the range reported by most flux sites (Wilson et al., 2002), providing additional confirmation of the turbulent flux quality (Moncrieff et al., 2004).

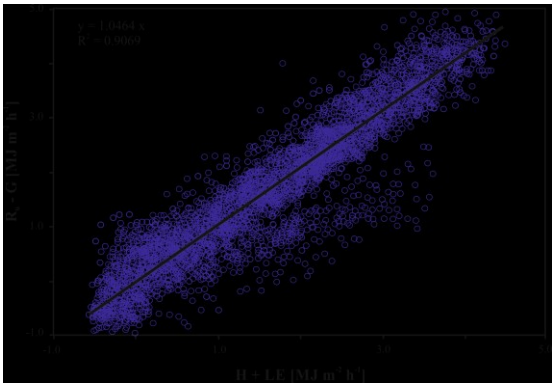

Figure 3.4 Energy balance closure at Case study 1

Hourly ET measurements by EC and transpiration fluxes measured during ERT experiment are shown in Figure 3.6.

3.5.2 Small scale ERT results and soil root-dynamics

The ERT monitoring produced two clear results:

- the initial conditions (11:00 a.m. of October 2, before irrigation starts) around the tree showed a very clear difference in electrical resistivity in the top 0.4 m of soil with respect to the rest of the volume (**Errore. L'origine riferimento non è stata trovata.**). Specifically, the resistivity of the top layer ranged around 40-50 Ohm m, while the lower part of the profile was about one order of magnitude more conductive (about 5 Ohm m). As no apparent lithological difference was present at 40 cm depth (see also laboratory results below) we attributed this difference to a marked difference in soil moisture content. This was confirmed by all following evidence (see below);

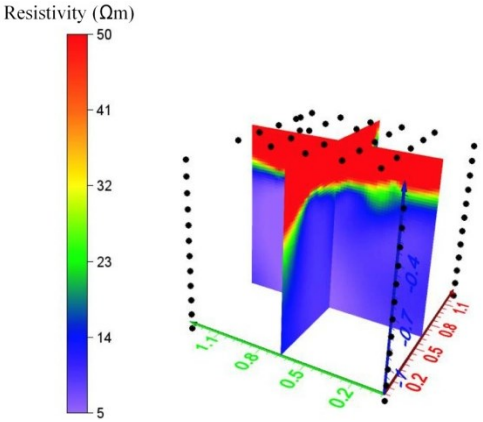

Figure 3.5 Cross sections of the ERT cube corresponding to the background acquisition (initial conditions) (from Cassiani et al., 2015)

- the resistivity changes as a function of time, during the two irrigation periods, during the night interval, and afterwards, all show essentially the same pattern, with relatively small (but still clearly measureable) changes (Figure 3.6). Two zone were identifiable: (a) a shallow zone (top 0.1-0.2 m) where resistivity decreased with respect to the initial condition; and (b) a deeper zone (0.2-0.4 m) where resistivity increased.

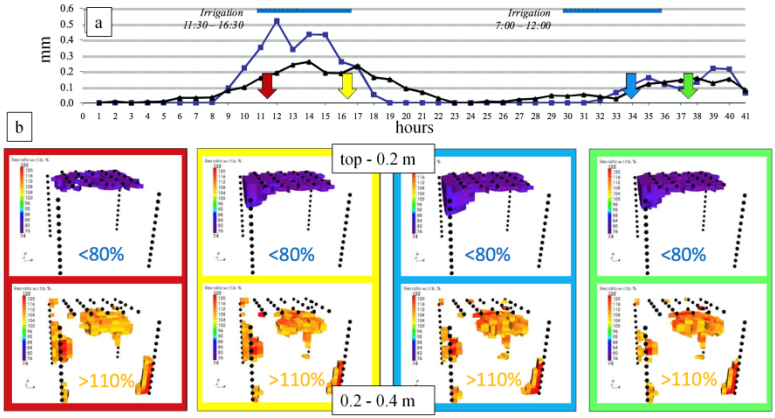

Figure 3.6 Hourly transpiration by sap flow (black line) and ET by EC (blue lines) fluxes measured at Case study 1, (a). 3-D ERT images of resistivity change with respect to background at selected time instants

Qualitatively, both pieces of evidence can be easily explained in terms of water dynamics governed by precipitation, irrigation and root water uptake. Specifically, the shallower high resistivity zone in **Errore. L'origine riferimento non è**

stata trovata. can be correlated to a dry region where root water uptake manages to keep soil moisture content to minimal values, as an effect of the entire summer strong transpiration drive.

The dynamics in Figure 3.6, albeit small compared to the initial root uptake signal in **Errore. L'origine riferimento non è stata trovata.**, still confirmed that the top 0.4 m was house to a strong root activity, to the point that irrigation cannot raise electrical conductivity of the shallow zone (0.1-0.2 m) by no more than some 20%, and the roots managed to make the soil even drier (with a resistivity increase by some 10%) in the 0.2-0.4 m depth layer (Figure 3.6). Note that, in general, resistivity changes of the type here observed cannot be uniquely associated to soil moisture content changes, as pore water conductivity may play a key role (e.g. Boaga et al., 2013; Ursino et al., 2014). However, in the particular case, hand care was taken to analyze the electrical conductivity of both the water used for irrigation and the pore water, purposely extracted at about 0.5 m depth. Both waters showed an electrical conductivity value in the range of 1300 μS/cm (thus fairly high, fact that explains the overall small soil resistivity observed at the site). Therefore, in this particular case we excluded pore water conductivity effects in the observed dynamics of the system. We tested soil samples, collected at Case study 1 site, in the laboratory of the Department of Geoscience (Padua University, Italy) to obtain a suitable constitutive relationship linking soil

moisture and electrical resistivity, given the know pore-water conductivity that was reproduced for the water used in laboratory. We conducted all measurements using cylindrical Plexiglas cells (Figure 3.7a) equipped with a four-electrode configuration designed to allow for sample saturation and de-saturation with no sample disturbance, using an air injection apparatus at one end and a ceramic plate at the opposite end. The air entry pressure of the ceramic is 1 bar; thus, during all the experiments the plate remained under full water saturation, while allowing water outflow during de-saturation. At each de-saturation step, we measured the electrical conductivity of samples under temperature-controlled conditions using a ZEL-SIP04 impedance meter (Zimmermann et al., 2008). A completed description of the laboratory set-up is given by Cassiani et al. (2009).

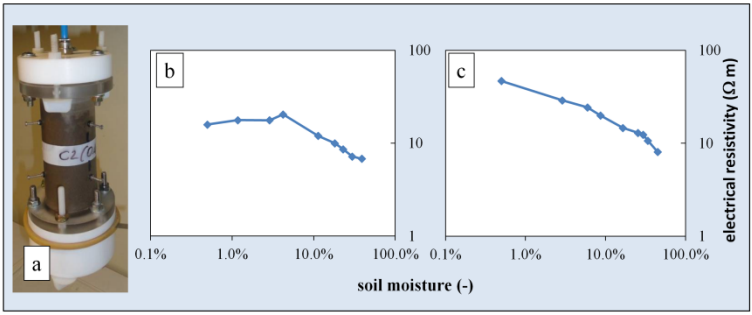

Figure 3.7 Lab-experimental relationships between electrical resistivity and soil moisture of samples (a) collected at 0.4 m (b) and 0.6 m (c) below the ground at Case study 1 site

Figure 3.7b and Figure 3.7c show two example experimental results on soil samples from two different depths (0.4 and 0.6 m below the ground, respectively). Note how in a wide range of soil moisture content (roughly from 5% to saturation) the two curves in Figure 3.7b and Figure 3.7c lied practically on top of each other. The same applied for all tested samples. Note also that, even though some soil samples show the effect of the conductivity of the solid phase (through its clay fraction) at small saturation (see sample from 0.4 m in Figure 3.7b) still the effect was small as it appears only at soil moisture smaller than 3-4%.

Therefore we deemed it unnecessary to resort to constitutive laws that represent this solid phase effect, such as Waxman and Smits (1968) that has been used for similar purposes elsewhere (e.g. Cassiani et al., 2012) and we adopted a simpler Archie's (1942) formulation. Consequently, we translated electrical resistivity into soil moisture using the following relationship calibrated on the laboratory data, using a water having the above mentioned electrical conductivity:

$$\theta = \frac{4.703}{\rho^{1.12}} \qquad (3.1)$$

where θ is volumetric soil moisture (dimensionless) and ρ is electrical resistivity (in Ohm m).

The relationship (Eq 3.1) allowed a direct translation of the 3D resistivity distribution to a corresponding distribution of volumetric soil moisture content.

3.5.3 Root water uptake modelling

ERT data were analysed as a function of depth, lumping the data horizontally by averaging estimated soil moisture along two-dimensional horizontal planes. ERT field evidence both in terms of background (**Errore. L'origine riferimento non è stata trovata.**) and time-lapse evolution (Figure 3.6) of soil moisture confirmed the hypothesis that, within the control volume, the distribution of water in the soil was largely one-dimensional as a function of depth. The data, once condensed in this manner, lend themselves more easily to a comparison with the results of infiltration modeling.

We implemented a one-dimensional finite element model based on a Richards' equation solver (Lin et al., 1997), simulating the central square meter of the ERT monitored control volume, down to a total depth of 2 meters (much below the depth of the ERT boreholes), where we assumed that the water table was located. Only the central part of the ERT-controlled volume (1 m x 1 m) was considered thus excluding the regions too close to the boreholes that, even though benefitting from the best ERT sensitivity, might have been altered from a hydraulic viewpoint by the drilling and installing operations. Correspondingly, the ERT data were averaged horizontally only in this central region. A very fine vertical discretization (0.01 m) and time stepping (0.01 h) ensures solution stability. The porous medium was homogeneous along the column and parameterized according

to the van Genuchten (1980) model. The relevant parameters had been derived independently from laboratory and field measurements, the latter particularly relevant for the definition of a reliable *in situ* saturated hydraulic conductivity estimate. The parameters used for the simulations were: residual moisture content $\theta_r = 0.0$; $\theta_s=0.54$; $\alpha' = 0.12$ 1/m'; n = 1.6; $K_s = 0.002$ (m h^{-1}). The remaining elements of the predictive modelling exercise were initial and boundary conditions. As we focused primarily our attention on reproducing the state of the system at background conditions, we set the start of the simulation at the beginning of the year (2013/1/1), and we assumed for that time a condition drained to equilibrium. Given the van Genuchten parameters we used and the depth of the water table, this corresponds to a fairly wet initial condition. We verified a posteriori that moving the initial time back of one or more years did not alter the predicted results at the date of interest (October 3, 2013). The dynamics during the year were sufficient to bring the system to the real, much drier condition in October. The forcing conditions on the system were all known: (a) irrigation was recorded, and only one dripper pertains to the considered square meter; (b) precipitation was measured; (c) sap flow was measured. Direct evaporation from the square meter of soil around the stem was neglected, considering the dense canopy cover and the consequent limited radiation received. Only one degree of freedom was left to be calibrated, i.e. the volume from which the roots uptake water. The thickness of the active root zone was estimated from the time-lapse observations (Figure 3.6), and fixed to the top 0.4 m after checking that limiting the root uptake to the 0.2 m to 0.4 m zone would produce results inconsistent with observations in

the top 0.2 m. Therefore only the surface area of the root uptake zone remained to be estimated. The predictive model was used as a tool to identify the extent of this zone, which is of critical interest also for irrigation purposes.

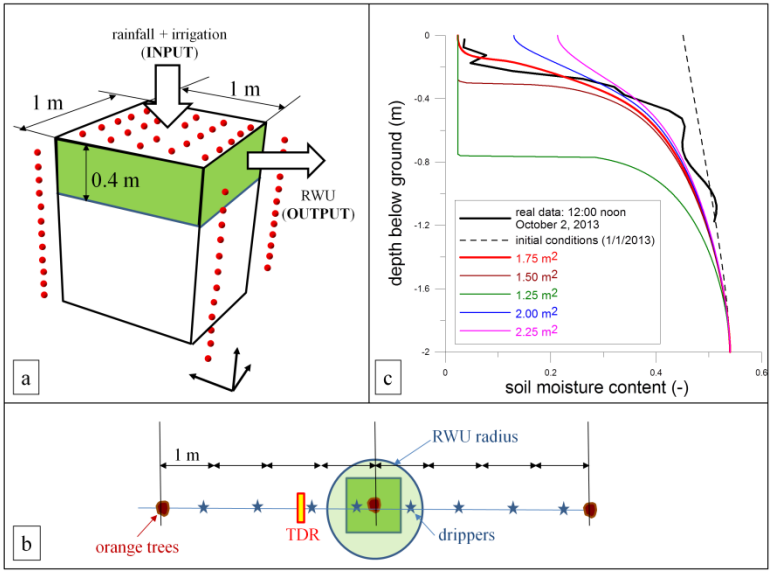

Figure 3.8 Conceptual 1-D Richards' equation model (a); results of 1-D Richards' equation simulations (b); the area that allows one to match the observed real profile with good accuracy (c) (modified from Cassiani et al., 2015)

Figure 3.8 shows the results of the calibration exercise. It was apparent that the total areal extent of the root uptake zone had a dramatic impact on the predicted soil moisture profiles, as it scaled the amount of water subtracted from the monitored square meter considered in the calibration. Even relatively,

small changes (+/-15%) of the root uptake area produced very different soil moisture profiles.

The value that allowed a good match of the observed profile was 1.75 m^2, while for areas equal to 1.5 m^2 and 2 m^2 the match was already unsatisfactory, leading respectively to underestimation and overestimation of the moisture content in the profile. Another important fact that is apparent from Figure 3.8. The estimated soil moisture in the shallow zone (roughly down to 0.4 m) was very small as an effect of root water uptake. However this dry zone must have a limited areal extent (1.75 m^2, corresponding to a radius of about 0.75 m from the stem of the tree). Indeed this was indirectly confirmed by the soil moisture evolution measured by TDR. Figure 3.9 shows the TDR data from three probes located about 1.5 m from the monitored tree (thus outside our estimated root uptake zone). The signal coming from the irrigation experiment of October 2, 2013 was very apparent with an increase in soil moisture of all three probes, located at different depths. Note that before this experiment the system had been left without irrigation for about two weeks. The corresponding effect on the TDR data was apparent: all three probes show a decline of moisture content during the day, with pauses overnight. The decline was more pronounced in the 0.35 m TDR probe, that lied at a depth we estimated to be nearly at the bottom of the RWU zone, and less pronounced above (0.2 m) and below (0.45 m). Note also that the TDR probes were close to another dripper, lying outside of the ERT controlled volume (the drippers are spaced 1 m along the orange trees line, with the trees about 4 m from each other) thus they reflected directly the infiltration

from that dripper. However, at all three depths the moisture content was much higher than measured in the ERT-controlled block closer to the tree. This can be explained with the fact that in that region the RWU was minimal or totally absent, while the decline of moisture content in time may well be an effect of water being drawn to the root zone by lateral movement induced by the very strong capillary forces exerted by the dry fine grained soil in the active root-zone closer to the tree.

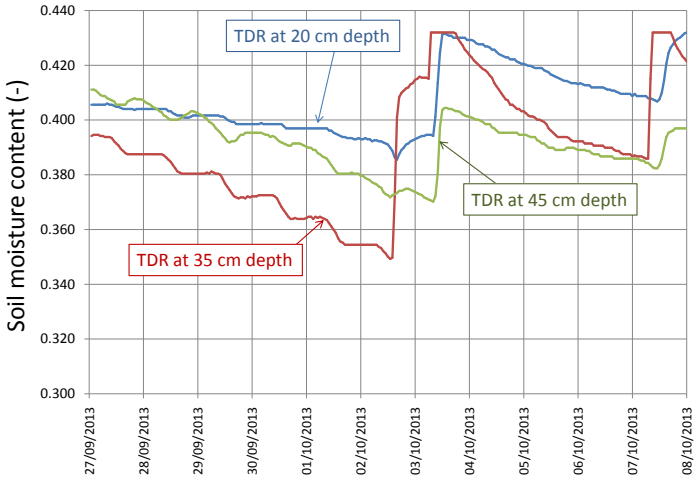

Figure 3.9 Hourly soil moisture from three TDR probes located about 1.5m from the ERT-monitored tree (from Cassiani et al., 2015)

The Case study 1 present a methodology based on coupling innovative data collection and models in order to obtain

quantitative estimates of the key parameters of such complex flow system. In particular we propose the use of hydro-geophysical monitoring via time-lapse electrical resistivity tomography (ERT) in conjunction with measurements of plant transpiration via sap flow and evapotranspiration (ET) from eddy covariance (EC).

The time-lapse 3-D ERT application conducted around the root-zone of a orange tree demonstrated the feasibility of the technique and its ability to monitor the RWU processes in terms of soil moisture variations due to distribution of active roots. Moreover the abundance of data (irrigation, precipitation, sap flow, ET data, soil hydraulic properties) collected at Case study 1 were used to calibrate a 1-D Richards' equation model representing the dynamics of the volume monitored via 3-D ERT..

The results of the calibrated modelling exercise allow for the quantification of the soil volume interested by RWU. This volume is smaller (with a surface area less than $2m^2$, and about 0.4 m thick) than expected and assumed in the design of classical drip irrigation schemes that prove to be losing at least half of the irrigated water which is not taken up by the plants.

Chapter 4

Case study 2

Case study 2

This Chapter describes an experimental application (Case study 2) corresponding to the joint use of ERT and sap flow transpiration data to characterize the soil volume of orange tree root-zone supplied by different irrigation techniques.

The results of this Chapter have been submitted to Journal of Hydrology by Vanella D., Consoli S., Cassiani G., Busato L., Boaga J., Barbagallo S., Binley A.

4.1. Field site description

The small scale 3D-ERT monitoring was conducted in an orange orchard (*Citrus sinensis* (L.) Osbeck) located in eastern Sicily – South Italy (37°20' N, 14°53' E, Figure 4.1), during the 2015 irrigation season. The grove belongs to the Citrus and Mediterranean Crops Research Centre of the Italian Council for Agricultural Research and Agricultural Economics Analyses (CREA-ACM, Acireale). 8-years old trees are spaced 4 meters within the trees row and 6 meters between the trees row, with mean leaf area index (LAI) and PAR light interception of 4.5 m^2 m^{-2} and 75%, respectively (Consoli et al., 2016 b). The climatic conditions prevailing at the experimental site (global radiation, relative humidity, wind speed and direction, air temperature) were measured and logged hourly using an automatic meteorological station installed close to the experimental orchard and surrounded by grass. The climate of the region is semi-arid Mediterranean,

with warm and dry summers. The 2015 irrigation season (from June 5 to October 12) was fairly dry, with total rainfall of about 100 mm (from a few episodic events). The evaporative demand of the atmosphere (reference evapotranspiration rate, ET_0) during the investigated irrigation season was of 697 mm, the average daily temperature was around 25°C (±5.8°C), with relative humidity of 70% (±26%). The maximum daily temperature recorded at the experimental site sometimes reached 40°C.

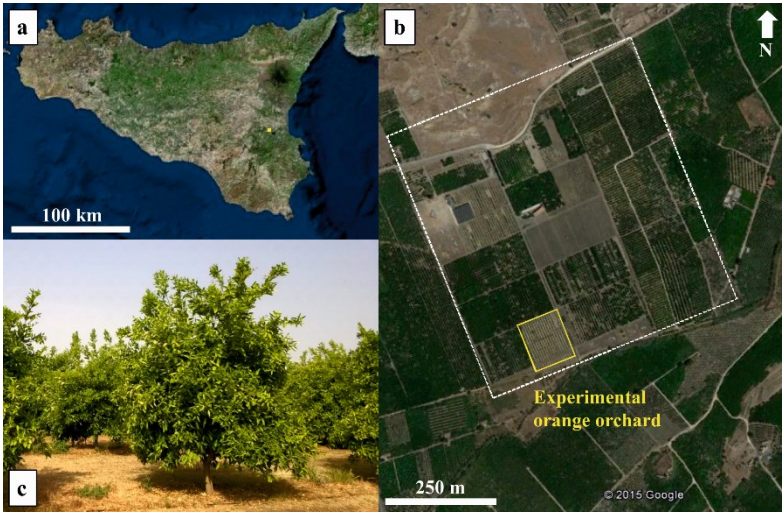

Figure 4.1 Location of the experimental site in Sicily (Italy) (a); experimental orange orchard (b); orange trees at the study site (c)

The soil at the experimental field is fairly uniform (in the top 0.1 m) with a sandy-loam texture (69.7 % of sand, 10.5 % of clay and 19.8 % of silt) and a percentage of organic matter of

1.25%. The mean water content at the field capacity (pF = 2.5) and wilting point (pF = 4.2) were 28% and 14%, respectively. The bulk density is about 1.32 g cm-3 (Consoli et al., 2014; 2016 b). Further analyses of texture and bulk density were conducted on soil samples collected also at different depths of the soil profile (i.e., 0.2, 0.4, 1.0 m). Irrigation water had medium salinity (EC25°C of 2.02 dS m^{-1}), alkaline reaction, and a pH of 7.30.

Irrigation rates were fixed on the basis of crop evapotraspiration (ET_c), eventually adjusted by rainfall. ET_c was calculated by multiplying the reference ET (ET_0), obtained by the Penman-Monteith approach (Allen et al., 1998; Allen et al., 2006) by the seasonal crop coefficient (K_c) for orange orchard, (i.e., 0.7 according to FAO-56). ET_c was further adjusted for a reduction coefficient, which depends on the canopy size with respect to the area pertaining to each tree (within the row and the corridors between the rows) in the field (Consoli et al., 2014). During June-October 2015, irrigation was supplied to the orchard three times per week, early in the morning. Two different irrigation regimes were tested in this study: (i) a control treatment (called T1), with trees irrigated with enough water to replace 100% of the ET_c, and (ii) a partial root-zone drying (PRD) treatment (called T4), with trees irrigated at 50% of the ET_c level, alternatively on either side of the root-zone, while the other side was kept dry. At the end of the irrigation season 2015, the amount of irrigation water applied to the full irrigation treatment (T1) was 266.4 mm and that applied to the PRD (T4) treatment was 158.2 mm, with a percentage of water saving of about 41%.

Trees of the two treatments (T1 and T4) were drip irrigated using two surface lateral pipes (located about 0.3 m far from the trunk line) per tree row; each lateral consists of six 4 L h^{-1} emitters (spaced 0.62 m) per tree. In T4, irrigation was applied only to one lateral pipe and the system was switched to the other fortnightly. T1 and T4 treatments are arranged in a randomized block (about 600 m^2 for each treatment in a total area of 0.5 ha) design, with three replicates for treatment, each consisting of three rows of 8 trees per row for a total of 24 trees (Figure 4.2).

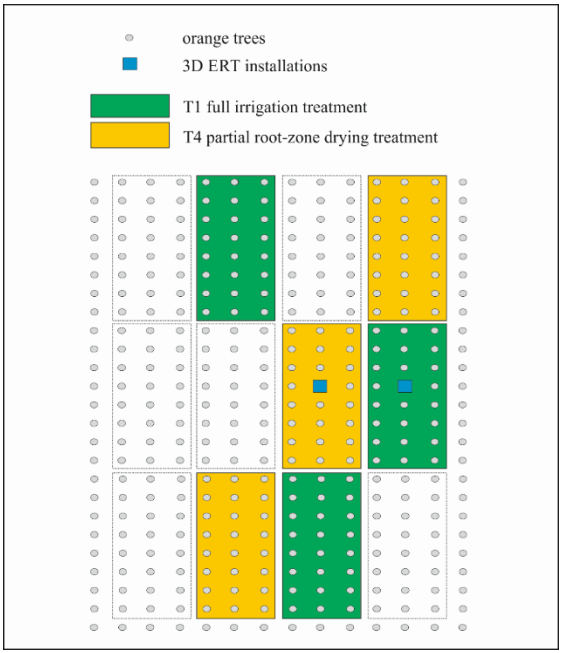

Figure 4.2 Irrigation treatments (T1, full irrigation and T4, PRD) at the experimental field. The blue circles identify the small scale 3-D ERT installations

The dynamics of soil water content (SWC; m^3 m^{-3}) distribution were monitored using soil moisture sensors (ECH2O probe, Decagon, Inc.) calibrated against the gravimetric method. Sensors were installed at a depth of 0.3 m from the soil surface. In the T4 treatment, soil moisture probes were installed at both eastern and western side of the trees trunk to provide information on water dynamics of the two sides of the root-zone system.

At the experimental site, the soil temperature was measured by soil thermocouple probes (TVAC, Campbell Sci.) located at 0.1 and 0.8 m below the soil surface. The soil temperature variations were, on average, 2°C during the ERT acquisitions period. Considering that the electrical resistivity is influenced only by 2% from temperature changes of 1°C (Friedman, 2005), in our case the temperature effect was neglected because it was low compared to SWC induced changes (Nijland et al., 2010).

4.2 Small scale 3D-ERT monitoring

The small scale 3-D ERT monitoring was conducted around two selected orange trees irrigated at full level (T1) and by PRD (T4), respectively (Figure 4.3).

4.2.1 Small scale 3D-ERT setup

The small case 3-D ERT set-up was an expanded version of previously tested schemes (Boaga et al., 2013; Cassiani et al., 2015; Cassiani et al., 2016; Consoli et al., 2016 b), using both superficial and buried electrodes for a three-dimensional electrodes arrangement.

The 3-D ERT setup (Figure 4.3) consisted of nine micro-boreholes (1.2 m depth, the green circles in Figure 4.3) housing 12 electrodes each (vertically spaced 0.1 m), plus 96 surface electrodes (spaced 0.26 m on a regular square grid). For each treatment (Figure 4.3, panels a and b), the boreholes are spaced 1.3 m on a square grid, thus delimiting four quarters (named C1-C2-C3-C4 and Q1-Q2-Q3-Q4 for T1 and

T4 treatments, respectively), only one of which is centred on the tree (C4 for T1 and Q4 for T4).

The small scale 3-D ERT monitoring was carried out both with long-term periodicity and short-term repetitions within the irrigation season (from June to September 2015). The main goal of this monitoring was the identification of the RWU patterns detectable, in principle, from changes in SWC, which in turn are detected as electrical resistivity changes in the ERT 3D images (e.g. Cassiani et al., 2016). The 3-D ERT long-term monitoring was performed at selected times of the irrigation season 2015, as follows:

- first monitoring: ERT1, June 8th-10th (pre-irrigation period);
- second monitoring: ERT2, July 14th-17th (one month after the beginning of the irrigation);
- third monitoring: ERT3, September 21st-24th (irrigation end).

During ERT2 and ERT3, time-lapse 3-D ERT repetitions (i.e., short-term monitoring) were performed in both T1 and T4 treatments, before (background measurements, i.e., corresponding to initial conditions) and after the irrigation event. For the plot quarters containing the trees (C4 and Q4, Figure 4.3), time-lapse 3-D ERT acquisitions were also performed during irrigation. These 3D-ERT short-term repetitions were performed in order to capture the RWU patterns at an hourly scale.

During the ERT acquisitions, continuous transpiration sap flows of the monitored trees (those falling in C4 and Q4) were

recorded. A total of 48 datasets were collected. Each dataset was acquired (quarter by quarter, using 72 electrodes at the same time) by adopting a complete 'skip 0' dipole-dipole scheme, (i.e., a configuration where the current dipoles and potential dipoles are both of minimal size, and they consist of neighbouring electrodes along the boreholes or at the surface). This setup ensures maximum spatial resolution (as good as the electrode spacing in the neighbourhood of electrodes). One disadvantage of the skip 0 dipole-dipole array is the poor signal-to-noise ratio at large separations between potential and electrode pairs (Binley and Kemna, 2005), but this issue is not crucial at the small scale considered here.

A ten-channel resistivity meter (Syscal Pro 72 Switch, IRIS Instruments) was used to collect the ERT data. A pulse duration of 250 ms for each measurement cycle and a target of 50 mV for potential readings were set as criteria for current injection. The sequence was optimized to take full advantage of the ten physical channels available for the instrument. The contact resistances of the electrodes were checked to ensure their suitability to inject current and to measure potential differences. Most of the electrodes were in excellent contact with the ground, even when the soil was relatively dry. Direct and reciprocal resistance data were acquired to have an estimate of measurement errors (see e.g., Binley et al., 1995; Daily et al., 2004). The dataset of each time step acquisition was made up of 4,885 values (both direct and reciprocal measurements), each survey lasted 25 minutes. At the same time of the small scale 3-D ERT monitoring, we extracted the soil pore solution (in T1 and T4) using ceramic suction

lysimeters (Soil Solution Access Tube, SSAT by IRROMETER Company, Inc.) posed at 0.30 m from the soil surface. The water pore electrical conductivity was measured in laboratory by a conductivity meter (HD2106.2, delta OHM Italy). The electrical conductivity of the irrigation water was also monitored.

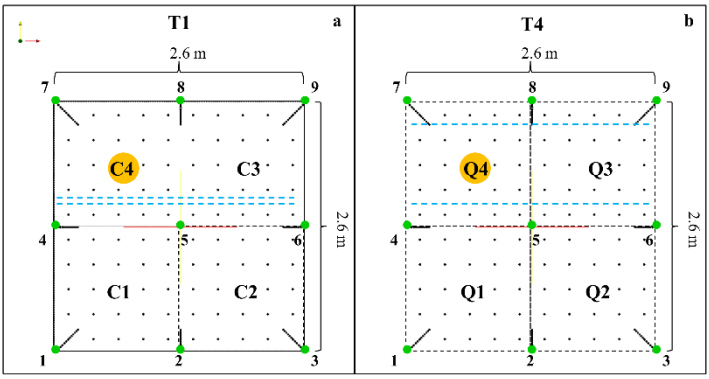

Figure 4.3 Small scale 3-D ERT monitoring scheme for T1 (a) and T4 (b) treatments. The orange circle represents the trees trunks falling in the quarters C4 and Q4; the black points are the superficial and buried electrodes; the blue dot lines indicate the irrigation pipelines in T1 (a) and T4 (b) treatments

4.2.2 Small scale 3D-ERT data processing

The protocol adopted to process each set of 3-D ERT data consists of the following steps:

1. identification of the reciprocal error (i.e., errors defined between the direct and reciprocal measurements collected *in situ*) according to Binley et al. (1995);
2. determination of geometric factor (K), that depends on the adopted electrode configuration (i.e., dipole-dipole skip 0);
3. renumbering of all electrodes in order to include them in the overall 3D inversions (see, step 7 of this list);
4. checking and averaging the duplicates measurements common to adjacent quarters;
5. building of the 3-D unstructured mesh. Unstructured tetrahedral meshes were generated by using the Gmsh software (http://geuz.org/gmsh/, Geuzaine and Remacle, 2009). The mesh adopted for the inversions was selected on the basis of the forward model performance (in terms of percentage error, see Eq. 1) and considering the modelling computation time. Unstructured tetrahedral meshes were preferred instead of structured triangle prism discretization for their capacity to enhance the computational efficiency. We preferred the adoption of unstructured meshes also because one advantage in their use is the facilitation of refining grids within distinct regions (outer and inner zones). The selected unstructured mesh contained two domains: an outer and an inner zone. The outer zone was composed of 79,529 tetrahedral elements and 12,551 node points. The depth of outer zone was 15 meters (12.5 times greater than the inner zone depth). The inner zone had 57,000 elements and 10,527 nodes;
6. assessment of the forward model errors, with the purpose of evaluating the accuracy of the numerical solution

(model error), the forward model error distribution was evaluated by testing different meshes. Specifically, forward models on a homogenous earth structure were performed for a series of unstructured discretization (meshes). Forward model percent error was calculated as follows:

$$\frac{\rho_\alpha - \rho_m}{\rho_\alpha} \cdot 100 \qquad (4.1)$$

where ρ_a is the apparent resistivity for a homogenous earth structure and equals to 100 Ω m; ρ_m is the calculated ρ_a by the forward model;

7. overall inversion of the dataset (background, acquired before the irrigation start and the dataset collected after the irrigation end) in absolute mode using the R3 code (Binley, 2013) with error level fixed at 10% and 16%;
8. overall inversion of the dataset considering all quarters together (Figure 4.3, including in the inversions all electrodes, i.e., buried and superficial) in relative mode (error level fixed at 10%). The relative inversion (also called time-lapse resistivity ratio inversion) was calculated as the ratio between the considered time step (e.g., during irrigation and after irrigation end) and the background dataset (i.e., initial condition) acquired before the irrigation start, as follows:

$$d_r = \frac{d_t}{d_0} \cdot F(\sigma_{\text{homog}}) \qquad (4.2)$$

where d_r is the resistance ratio, d_t e d_0 are the dataset collected at the time (t) and at the initial condition (0), and $F(\sigma_{homog})$ is resistance value obtained by running the

forward model for an arbitrarily chosen conductivity (100 Ωm). The time-lapse resistivity ratio imagery show the changes in percentage terms, caused by irrigation and RWU, relative to this reference value;

9. time lapse inversions of the quarters containing the trees (Q4 and C4, Figure 4.3) again using Eq. (4.1), with the error level fixed at 5%.

4.3. Transpiration measurements at tree level

Water consumption at tree level was continuously measured using the heat pulse velocity (HPV) sap flow technique (Swanson and Whitfield, 1981). Two trees for each treatment (T1 and T4) were selected to measure plant sap flow. The HPV technique is based on the measurement of temperature variations (ΔT), produced by a heat pulse of short duration (1-2 s), in two temperature probes installed asymmetrically on either side of a linear heater that is inserted into the trunk. For HPV measurements, one 4 cm sap flow probe with two thermocouples embedded (Tranzflo NZ Ltd., Palmerston North, NZ) was inserted in the trunks of the trees. The probe was positioned on the southern side of the trunk at 0.2 m from the ground and wired to a data-logger (CR1000, Campbell Sci., USA) for heat-pulse measurement and record; sampling interval was 30 minutes. The temperature measurements were obtained by means of ultra-thin thermocouples that, once the probe is in place, are located at 5, and 15 mm within the trunk. Data of the probe were processed according to Green et al. (2003) to integrate sap flow velocity over sapwood area for transpiration estimation. Specifically, the volume of sap flow in the tree stems per unit time was

estimated by multiplying the sap flow velocity by the cross sectional area of conducting tissue. For this purpose, fractions of wood (F_M=0.48) and water (F_L=0.33) in the sapwood were determined on the trees where sap flow probes were installed. In particular, FM and FL were measured in wood samples (5 mm diameter, 40 mm length) taken with an increment borer in the proximity of the probe sets. The calculation of FM and FL requires the input of fresh weight, oven-dried weight, and immersed weight (Si et al., 2009).

4.4. Results and discussion

4.4.1 Soil water content dynamics during the small scale 3-D ERT monitoring

Figure 4.4 shows the irrigation rates supplied to T1 and T4 (eastern and western sides). The timing of small scale 3-D ERT monitoring (ERT1, ERT2 and ERT3) is also displayed in Figure 4.4 (yellow triangles with the labels) and refers to the months of June, July and September 2015. The results of the soil water content (SWC, m^3 m^{-3}) monitoring for PRD treatment (also in Figure 4.4) show the expected alternating drying and wetting cycles on either soil sides (i.e., East and West) after each switching event. In the T1 treatment, supplied at full rate of ET_c, the SWC remained close to the field capacity (i.e., 0.28 m^3 m^{-3}).

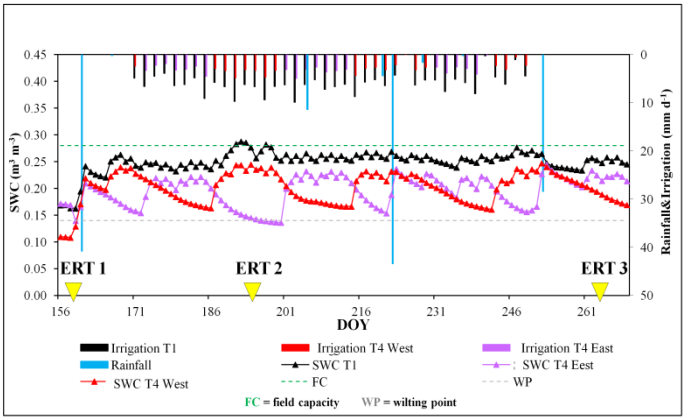

Figure 4.4 Daily evolution of soil water content (SWC, m^3 m^{-3}) measured by TDR in the PRD (T4) and the control treatment (T1) during the irrigation season 2015

Figure 4.5 shows the SWC dynamics at hourly basis recorded by TDRs during the small scale 3-D ERT monitoring. During ERT1 (Figure 4.4), at the beginning of the irrigation season (June 5th 2015, day of the year - DOY_S 159-160, Figure 4.5a), the SWC was well below the field capacity (i.e., 0.28 m^3 m^{-3}) in both T1 and T4 treatments, with values close to the permanent wilting point (i.e., 0.14 m^3 m^{-3}). A rainfall event of 23 mm (i.e., effective rainfall), occurred in DOY (day of year) 160, contributes to rise the SWC. During ERT2 (Figure 4.4), at the end of July (i.e., DOY_S 195-198, one month after the beginning of the irrigation), the SWC remained fairly close to field capacity in T1 and slightly lower than this in the T4 West side (Figure 4.5b), which had been switched on since the week before (Figure 4.4). Conversely, the SWC in T4

East side remained fairly steady and slightly higher than the permanent wilting point.

During the ERT3 survey, at the end of September, (i.e., DOY_S 264-267, irrigation season end, Figure 4.4), the SWC at T4 East and West sides presented very similar values, due to the alternating switching operation of the irrigation laterals, which have ensured good soil moisture conditions (0.18 and 0.22 m^3 m^{-3} respectively for T4 West and East), even under deficit irrigation.

The laboratory analysis of both soil pore solution and irrigation water indicated a moderate salinity, with EC_{25}°C values in the range of 2-3 dS m^{-1} (Rhoades et al., 1992). The observed variability of EC should not cause major alterations in ERT monitoring (Cassiani et al., 2016), thus resistivity variations can be considered as mainly related to changes in SWC. During the monitoring, the daily average transpiration fluxes (T_{SF}) reaches 1.9 mm d^{-1} in the fully irrigated treatment T1, and 0.9 mm d^{-1} in the T4 PRD treatment, compared to a rate of ET_c of 2.1 mm d^{-1}. During the hottest daily hours (i.e., from 12:00 a.m. to 04:00 p.m. LST), sap flow fluxes were fairly steady due to tree capacitance and physiological control mechanisms (Motisi et al., 2012).

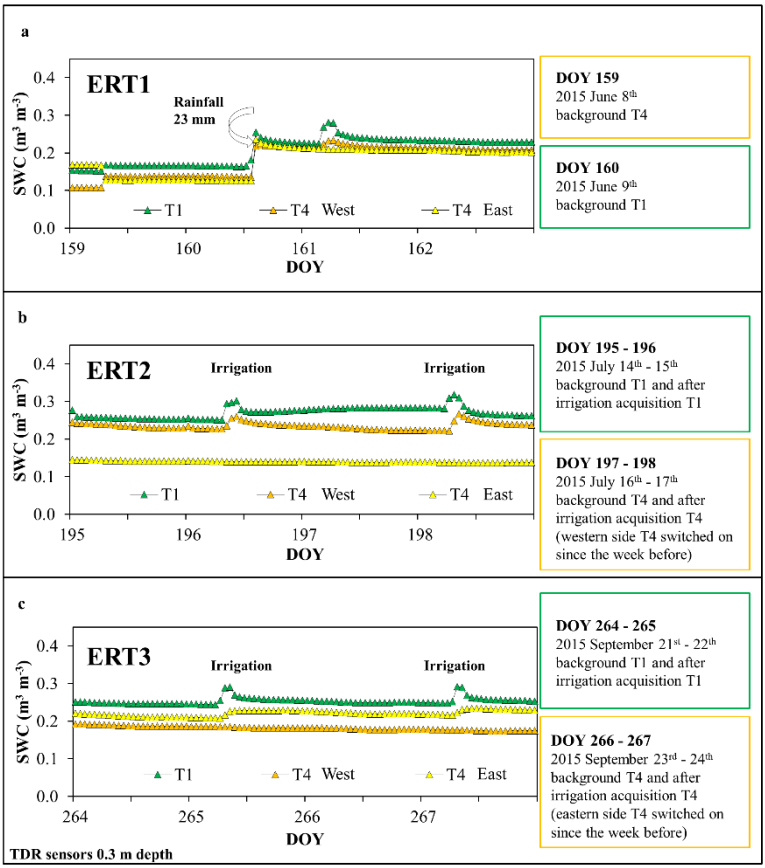

Figure 4.5 Hourly soil water content (SWC, m^3 m^{-3}) measured by TDRs during the 3-D ERT monitoring in 2015: June, ERT1 (a), July, ERT2 (b), September, ERT3 (c)

4.4.2 Small scale 3-D ERT results and soil-root dynamics

In the following, we describe in detail the results of the ERT geophysical monitoring, carried out during the irrigation season 2015 at the experimental treatments T1 and T4. Considering the quality of the ERT data, the average reciprocal errors for the whole quarters in T1 and T4 were respectively of 2.6% (±1%) and 2.9% (±0.9%). Overall, the data quality was considered to be excellent.

4.4.2.1 ERT results: long-term monitoring

The ERT dataset acquired during the long-term monitoring were analysed in absolute terms (i.e. considering one dataset only at the time). Most of these inversions converge after an acceptable number of iterations (6-8 iterations) at the error level of 10%. However, in some cases it has been necessary to raise the target error level above 10% to reduce the spatial variability of the obtained resistivity images. A couple of reasons can be called into play for this behaviour, namely: (1) a known disadvantage of the dipole–dipole scheme is the weak signal to noise ratio, and at large separations between current and potential electrode pairs (Binley and Kemna, 2005) this can become a serious issue; (2) especially under very dry conditions, the soil shows the presence of soil cracks and the gaps at the soil-root interface, that are easily to find around large structures (Carminati et al., 2009). Therefore, in some cases in order to obtain smooth images, we increased the assumed data error to 16%.

Table 1 reports the performance of the absolute model inversions (i.e., number of iterations to reach the solution,

number of data used in the inversion, computational time spent on, number of rejected data, final RMS misfit) for the chosen error level of 16%. The largest part of the dataset converged in less than five iterations. The time spent (seconds) is proportional to the number of quadripoles used in the inversions, which increases from ERT1 to ERT3, probably because the electrodes-soil contacts improved during the irrigation season due soil settling around the boreholes.

Figure 4.6 shows the inverted images (absolute inversions) of the background dataset (i.e., initial condition) collected during ERT1, ERT2 and ERT3 (panels a and b) in T1 and T4 treatments, with the electrical resistivity profiles averaged in selected soil layers (0.0 - 0.2 m; 0.4 - 0.6 m; 0.6 - 0.8 m; 0.8 - 1.0 m; 1.0- 1.2 m) of the investigated soil volume by the ERT technique (panels c and d). Values are expressed in terms of electrical resistivity (Ω m). The images are depth slices and the active irrigation pipes are represented using black solid lines. From the results of the long term ERT monitoring (Figure 4.6) different spatial and temporal patterns of electrical resistivity distribution are apparent within the investigated soil portions. Since soil texture at the investigated layers in T1 and T4 results quite homogeneous, with a prevalent sandy-loam composition (66.37± 2.06 % of sand, 20.92±3.52 %of silt, 12.72±1.02 % of clay), the observed electrical resistivity variations should depend, for the most part, on SWC changes that are caused by a combination of irrigation and RWU dynamics. Over time, from ERT1 (June) to ERT3 (September), there is a reduction of electrical resistivity, with an average variability from 59

(±31) to 18 (±4) Ωm in T1, and from 65 (±34) to 40 (±7) Ωm in T4. This is clearly a consequence of the adopted irrigation strategies (i.e. full versus deficit irrigation). At the end of the irrigation season (ERT3), in the entire monitored soil profile (0.0-1.0 m), the mean reduction of electrical resistivity was of 69% in T1 and of 38% in T4. In both treatments the greatest variability of electrical resistivity is found in the upper soil layer (0.0–0.2 m), with mean resistivity values varying from 118 to 16 Ωm in T1 and from 139 to 39 Ωm in T4, (Figure 4.6, panels c and d). This is most likely due to the adopted superficial micro-irrigation system and in the case of T4 (PRD) also due to the irrigation shift between either sides of the plant root system. Overall, the most notable features emerging from the absolute inversions in Figure 4.6 are the high resistivity areas located especially at depths between 0.4 and 1.0 m. These features are more clearly marked at the start of the irrigation season 2015 and are present in both T1 and T4. Their time evolution shows how these features are progressively smeared and reduced in magnitude, blending into the generally more conductive situation generated, both in T1 and in T4, by the following irrigation period. Even though smeared, the features are not erased in the following time steps and maintain their general structure. The resistivity anomalies have generally fairly high values (larger than 100 Ωm). This is particularly notable especially in presence of fairly conductive pore water (see above: 2-3 dS m^{-1}) that immediately calls for strong unsaturated conditions to give bulk electrical resistivity well above 100 Ωm, especially as these features change in time and are more intense during the drier soil conditions, before irrigation. How such very resistive features can exist at localized locations at depth is

not easy to explain if not calling into play local RWU that would be reasonably intense at depth during the long period of time (November to May) when the crops are not irrigated.

In order to summarise the general time-evolution of electrical resistivity as imaged by ERT box-plots are shown in Figure 4.7. Each box-plot splits the ERT data set (ERT1, ERT2 and ERT3) into quartiles and refers to the electrical resistivity distribution at specific depth intervals (0.0 – 0.2 m, panels a, d); (0.4– 0.6 m, panels b, e); (1.0– 1.2 m, panels c, f). Each box-plot extends from the first to the third quartile, showing the median values of each data set. Two vertical lines (whiskers) extend from the upper and lower part of the box. The lower whisker goes from first quartile to the smallest non-outlier in the data set, and the upper whisker goes from third quartile to the largest non-outlier. In the T1 treatment (Figure 4.7, panels a, b, c), the electrical resistivity medians decrease from ERT1 to ERT3 (i.e., from June to September 2015), and the spread around the median decreases significantly, pointing out at a more homogeneous resistivity pattern as irrigation takes place. This behaviour is in agreement with the increasing trend of the SWC distribution monitored (Figure 4.4 and Figure 4.5) through the irrigation season 2015. In contrast, in the T4 treatment (Figure 4.7, panels d, e, f) the electrical resistivity medians do not show a specific trend with time, neither in median or in spread, most probably due to the SWC heterogeneities related to the alternation of the irrigation phase, as required by the PRD technique, and to the smaller applied water volume.

Table 4.1 Summary of the performances of the total absolute inversion for ERT1 (a), ERT2 (b) and ERT3 (c) for both the treatments (T1 and T4), for absolute inversion error at 16%.

Survey	Treatments	Dataset	n. of iterations	initial n. of measurements	time spent on (s)	n. of rejected measurements	RMS
ERT1 (June)	T1	background	5	2077	6173	526	1.78
	T4	background	4	2043	5038	349	1.88
ERT2 (July)	T1	background	4	3695	11355	659	1.24
		after irrigation	4	3501	8284	609	1.12
	T4	background	5	3590	6027	717	1.06
		after irrigation	6	2833	7105	529	1.14
ERT3 (September)	T1	background	4	4067	10606	1024	1.21
		after irrigation	4	4408	10574	875	1.23
	T4	background	5	3342	11591	1001	1.17
		after irrigation	4	2900	5633	462	1.12

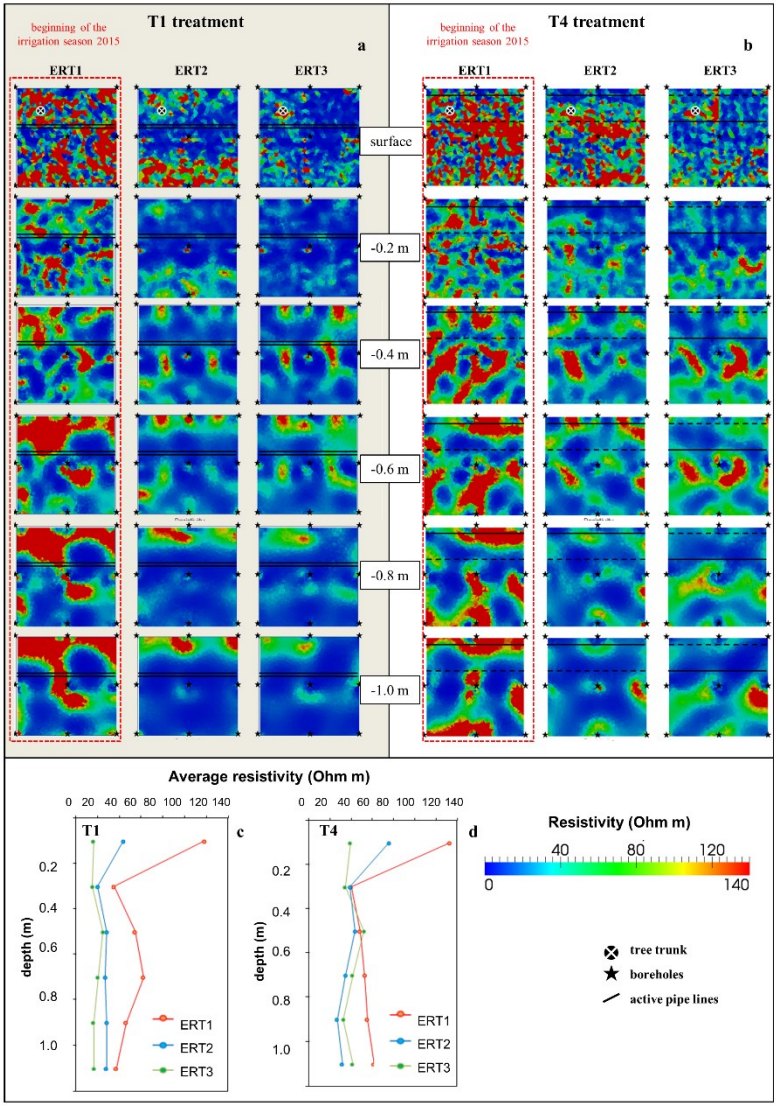
T1 treatment
beginning of the irrigation season 2015
a
ERT1
ERT2
ERT3
T4 treatment
beginning of the irrigation season 2015
b
ERT1
ERT2
ERT3
surface
-0.2 m
-0.4 m
-0.6 m
-0.8 m
-1.0 m
Average resistivity (Ohm m)
0 20 40 60 80 100 120 140
T1
c
depth (m)
0.2
0.4
0.6
0.8
1.0
ERT1
ERT2
ERT3
T4
Resistivity (Ohm m)
40
80
120
0
140
tree trunk
boreholes
active pipe lines

Figure 4.6 (previous page) Absolute inversions of the background datasets collected during the long-term ERT monitoring (ERT1, ERT2, ERT3, June-September 2015), in T1 (a) and T4 (b) treatments. Average resistivity values are reported in function of the depth (c, d)

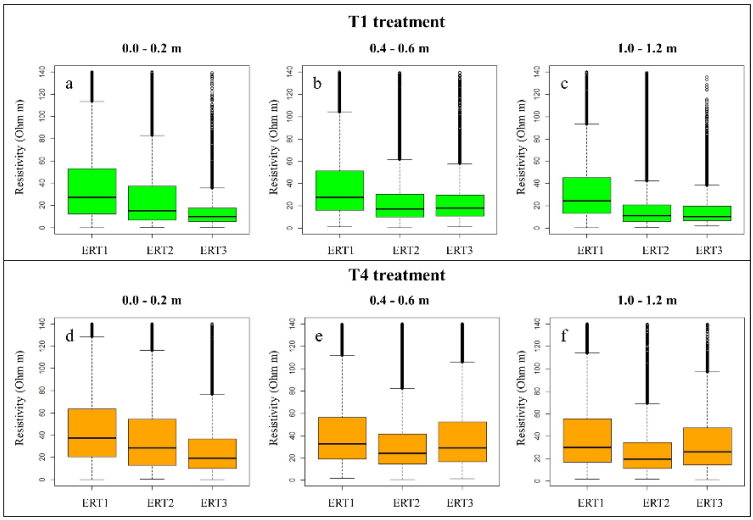

Figure 4.7 Box-plots of the electrical resistivity distribution in the different soil layers in T1 and T4

The results of the 3-D ERT long-term monitoring, at the beginning of the irrigation season 2015 (June), show greater resistivity anomalies along the volume of investigated soil. The resistivity positive anomalies (resistivity values higher than 100 Ωm) could be correlated to dry regions where RWU manages to keep SWC to minimal values. Eventually, the presence of a shallow water table should be verified in the

future applications. At the mid and at the end of the irrigation season (July and September) the resistivity anomalies in some cases migrated near the surface in proximity of the superficial emitters for both treatments. For Case study 2, our results have indicated a switch of tree water source from the deeper soil profile, at the beginning of the irrigation season, to shallow water source point, during the irrigation phase. In this context, resistivity images may give useful information on the description of the sub-soil dynamics that occur in the root-zone of the irrigated trees.

4.4.2.2 ERT results: short-term monitoring

The interpretation of the short-term time-lapse ERT monitoring is slightly more complex. Figure 4.8 shows the time-lapse ratios (in %) of resistivity at the end of irrigation over the resistivity before irrigation, in both T1 (panels a and b) and T4 (panels c and d) treatments. Note that the corresponding background conditions are shown in Figure 4.6.

In Figure 4.8, values of electrical resistivity ratio around 100% indicate no change from the background, while values higher or lower than 100%, correspond respectively to electrical resistivity increases (i.e., decrease in SWC) and decreases (increase in SWC). A quantitative translation of resistivity changes into SWC changes is possible, e.g. using classical Archie's law (1942) or more general empirical

relationships (e.g. Waxman and Smits, 1968, Brovelli and Cassiani, 2011). However in this study we limit ourselves to analysing the patterns of electrical resistivity as, given the homogeneity of pore water electrical conductivity in the time period of interest (summer, with very little direct precipitation), bulk resistivity and SWC are in a direct, monotonic relationship.

The images in Figure 4.8 present fairly complex patterns that are a result, as observed in similar studies (e.g. Cassiani et al.,2015 and 2016), by the concurring wetting effect caused by irrigation and the drying effect caused by RWU. This interaction is even more confusing when examining only the net ratio between the states before and after irrigation, as shown here, as the observed patterns are the cumulative effects of irrigation and evapotranspiration occurred in the entire time lapse. In addition, as discussed in section 3.2.1 above, there is evidence that the root structure in both treatments is complex, driven as it is by two different forcing conditions, acting in two different periods of the year: (1) the need to exploit in an optimal manner the water provided by irrigation, from June to September, thus pushing for the development of shallow roots active in the vicinity of the drippers, and (2) the need for the plant to retrieve water during the long non-irrigated period, and particularly during the Spring vegetative phase, and thus searching for water in the deeper part of the soil profile.

The conditions above produce patterns of increase and decrease in resistivity after irrigation that are apparently very complex to decipher. However, some clear phenomena are readable. In particular:

- as irrigation takes place in a very localized region of the broader area monitored by ERT, it is not surprising that resistivity tends to diminish largely in correspondence of the drippers and below them, creating very consistent patterns extending from the surface to the bottom of the monitored soil volume (approximately 1 m below ground);
- some areas, particularly at depth, show an increase in resistivity irrespective of the application of the irrigated water. This is not a strange phenomenon, as ET during the hotter times of the day well exceeds the amount of irrigated water, and the corresponding SWC is likely to be lower in the afternoon with respect to the early morning situation. The same was observed e.g. by Cassiani et al., (2015), also in an orange orchard (herein reported in Chapter 3). The peculiar characteristic of the dataset presented here is that some resistivity increasing areas are located at depth, where are located the deepest roots. In fact a comparison between the higher resistivity zones in Figure 4.6 (surveys ERT1) and the resistivity increase zones in Figure 4.8 shows that there is a remarkable correlation between the two;
- as the amount of applied water is larger in T1 than in T4, the phenomena tend to be more extreme in T1, especially in July when apparently the amount of water irrigated in T4

was totally transpired nearly at all depth (not very surprisingly in the hottest period of the year).

Figure 4.8 (next page) Time-lapse resistivity ratio in T1 and T4 during July (ERT2, panels a, c) and September (ERT3, panels b, d) respect to the corresponding background conditions

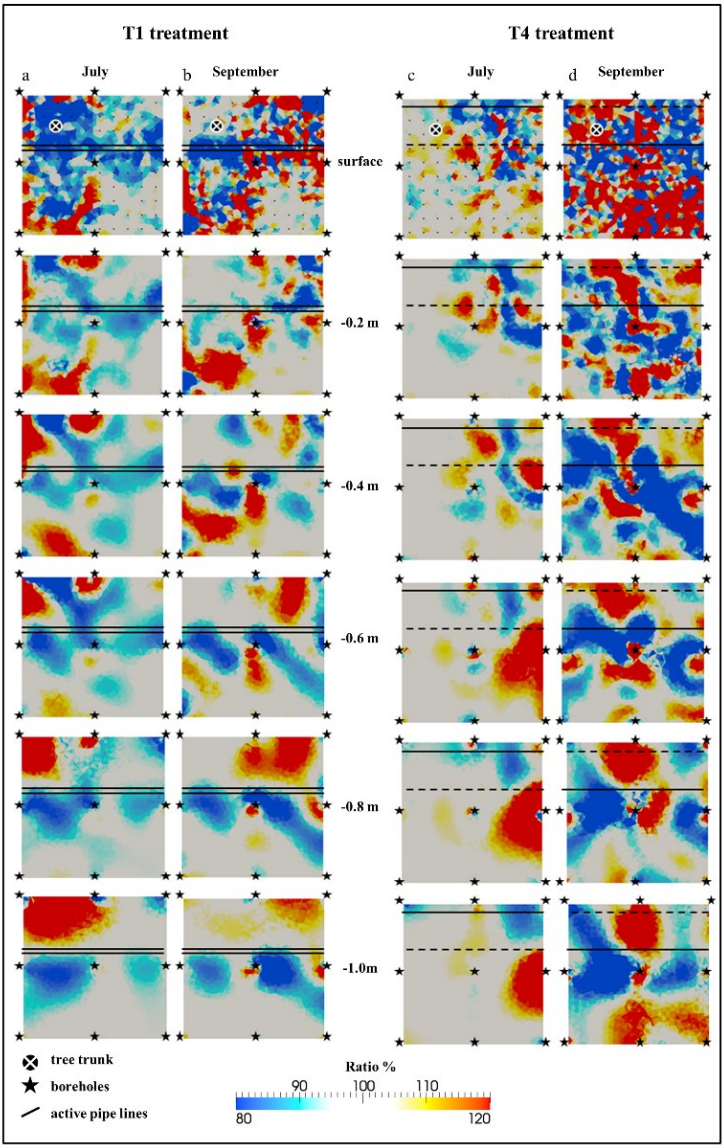
T1 treatment
T4 treatment
a
July
b
September
c
July
d
September
surface
-0.2 m
-0.4 m
-0.6 m
-0.8 m
-1.0m
tree trunk
boreholes
active pipe lines
Ratio %
80
90
100
110
120

4.2.2.3 ERT results: short-term monitoring at C4 and Q4 quarters

As noted above, the complexity of the time-lapse processes involved in the irrigation versus evapotranspiration balance cannot be fully ascertained just considering the cumulative changes occurred during the irrigation / evapotranspiration time. Therefore it is instructive to analyse the data that could be collected at a faster rate limiting the focus to only one quadrant of the four monitored at each treatment. In this manner, it was possible to replicate the time resolution experimented at other sites (see e.g. Cassiani et al., 2015 and 2016).

Figures 4.9 and 4.10 show the datasets for quadrants C4 and Q4 that contain the trees in the T1 and T4 plots, respectively. For these quadrants, ERT repetitions were performed before (time 00), after (time 03) and during (time01 and 02) the irrigation phase. The 3-D ERT short-term monitoring was able to capture the soil dynamics acting within the root zone of C4 and Q4. In Figures 4.9 and 10, the panel a shows examples of time-lapse resistivity ratio images for C4 and Q4, while panel b depicts the hourly transpiration fluxes (mm h^{-1}) of the irrigated tree under T1 and T4 treatments.

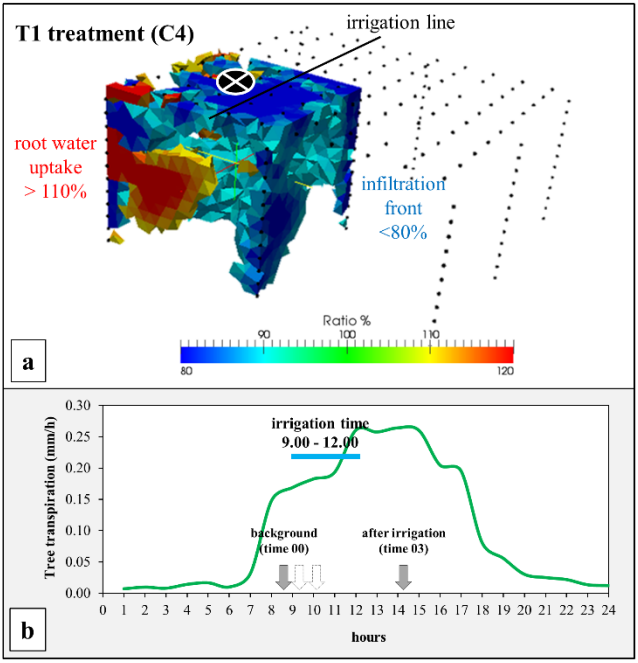

Figure 4.9 Time-lapse resistivity ratio volume at a selected time step (after the end of the irrigation, time 03) with respect to the background condition (before irrigation, time 00), a); Tree transpiration rate (mm h^{-1}), irrigation and ERT surveys timing are displayed in the graph in function of time, b). Data refers to the full-irrigated treatment (T1) on July 15, 2015

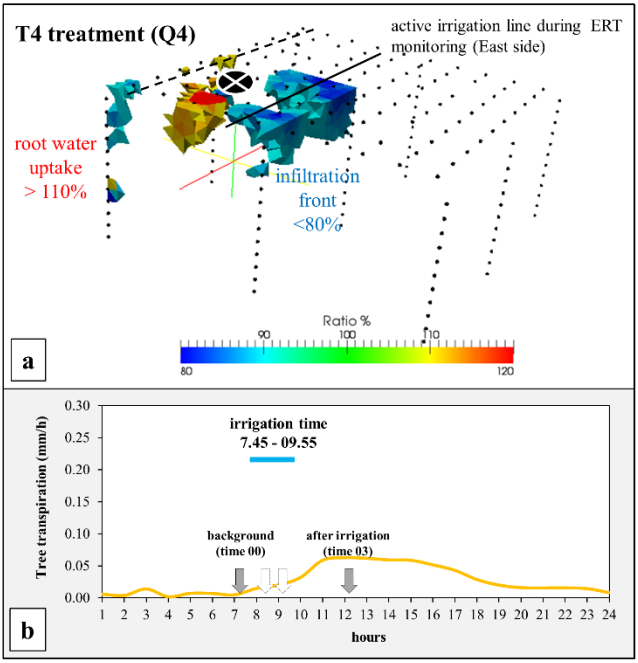

Figure 4.10 Time-lapse resistivity ratio volume at a selected time step (after the end of the irrigation, time 03) with respect to the background condition (before irrigation, time 00), a); Tree transpiration rate (mm h^{-1}), irrigation and ERT surveys timing are displayed in the graph in function of time, b). Data refers to the PRD treatment (T4) on September 24, 2015

Figure 4.9a refers to the resistivity ratio of the fully irrigated quarter (C4) in T1, at the end of the irrigation (time 03, 236 minutes after the beginning of the irrigation), on July 15th, 2015. This image shows a remarkable decrease in resistivity (over about 40% of the whole soil volume) with respect to the initial condition, as an effect of the soil wetting caused by the irrigation front. The decrease is observed, with decreasing intensity from the topsoil, close to the irrigation pipelines, down to a depth of roughly 1.2 m from the surface. In the upper soil layer (from the top to 0.2 m below the surface), a decrease in resistivity was already observed at previous time steps (time 01 and time 02, ERT dataset acquired during irrigation not showed here) close to the irrigation pipelines. Specifically, at time 01 (36 minutes after the start of the irrigation) the decrease in resistivity term involves 4% of the whole monitored volume and at time 02 (after 89 minutes since the beginning of the irrigation) 10% of the same volume. After the end of irrigation (time 03, Figure 4.9a), 7% of the whole C4 volume shows a resistivity increase. The maximum increase in resistivity terms is observed from 0.60 to 0.80 m depth of the soil profile, where the most root activity is expected to make the soil drier due to the RWU. At the same time (i.e., time 03, Figure 4.9b) the RWU rate was at a maximum, as observed by the transpiration fluxes (Figure 4.9b).

Figure 4.10a shows a time-lapse resistivity ratio image for the Q4 quadrant (T4) referred to the end of the irrigation (time 03, 283 minutes after the beginning of the irrigation), with respect to the initial condition (time 00, no irrigation) on September 24th, 2015. A slightly decrease in resistivity (in

average from 2 to 7 % of the whole Q4 quadrant volume) is detected with respect to the initial condition, in a position close to the active irrigation pipeline of the PRD system (T4 East). Specifically, the evolution of the water plume (Figure 10a) is well captured by the small scale 3-D ERT technique. The regions where resistivity changes (decreasing and increasing) are limited to the surrounding of the two drippers, and the water seems to infiltrate no more than 0.2–0.4 m below the soil surface (decrease in resistivity terms of 22% of the soil layer). In this upper soil layer, a decrease in resistivity terms was already observed in previous time steps (time 01 and time 02, ERT dataset acquired during irrigation, not showed here), close to the irrigation pipelines. At time 01 (47 minutes after the start of the irrigation) the decrease in resistivity involves 5% of the top soil layer (down to 0.4 m below the surface) and 13% at time 02 (after 93 minutes since the beginning of the irrigation). At time 03 (Figure 4.10a), a slightly increase in resistivity is detected (3% of the soil layer from the top soil to 0.40 m below the soil surface), that may be correlated to the RWU (Figure 4.10b), that is already much lower than the corresponding example in Figure 4.9.

4.4.3 Discussion

The ERT images interpretations may be affected by some uncertainties. In general, electrical resistivity changes of the type here observed could not be uniquely associated with SWC changes, because temperature and pore water conductivity (e.g., variations due to selective ions by RWU) may play a key role (Boaga et al. 2013; Ursino et al. 2014; Cassiani et al. 2016).

In our case, the continuous monitoring of soil temperature and the analysis of pore water conductivity show quite stable values during our experiment. Thus, the temporal and spatial patterns of electrical resistivity changes may be mainly ascribed to the SWC variations. Conversely, the SWC depletion in the investigated soil profile may be considered as an indicator of the root activity (Tenhunen et al., 2013). Therefore, in the investigated soil profile, water losses may be mainly attributed to evaporation and RWU processes. Evaporation is particularly significant in the top-soil (i.e. near the soil surface) but it is not a significant pathway for water losses from greater depths. Thus, water depletion from subsurface soil layers can be attributed to root activity. Plant roots transfer water between soil layers of different water potential thereby significantly affecting the distribution and availability of water in the soil profile (Burgess et al, 1998).

In this study, within the volume of the investigated sub-soil by the small scale 3-D ERT monitoring, the resistivity images shows significant differences in spatial and temporal terms, both in absolute (Figure 4.6 and Figure 4.7) and in relative terms (Figure 4.8, Figure 4.9, Figure 4.9). These changes could be related to the different responses of the active roots as a function of irrigation operations (timing and regime). Analysis of plant root systems, in terms of electrical proprieties, is difficult to identify under field conditions, especially in the trees root systems, which are large and complex and include fine absorbing roots as well as conducting coarse roots (Aubrecht et al., 2006).

Plant cells are relatively poor conductors of electric current because the cell walls have an electrical resistivity (specific

electrical resistance) equivalent to the resistivity of technical insulators of Class II (≈ 104–1010 Ωm). The sensitivity of the ERT technique to the presence of high resistivity materials constituted the base for the use of the technique for imaging woody plant root system (Amato et al. 2008; Rossi et al. 2011).

Some authors (among others, al Hagrey et al., 2007; Amato et al., 2010; Rossi et al., 2011) associated areas of larger resistivity with trees roots location. Rooted soil may be viewed as a complex of conductive soil volumes interacting with a resistive matrix, which is continuous and branched, and may be able to redirect the slow-down electrical charges because of its spatial arrangement more than to the actual occupied volume (Mancuso, 2012).

Quantitative research on the use of resistivity tomography for mapping root system spatial variability have shown that lignified coarse plant roots exhibit a strong electrical response, that rooted soil resistivity can increase several hundred Ω m (Amato et al. 2008). Amato et al., (2009) have shown that even at very low density of herbaceous roots can increase resistivity distribution, but the response in resistivity is of the same order of magnitude as the effects of grain size and water content, the latter being most likely to be responsible for the main resistivity variations observed e.g. in our Case study.

As reported in the literature (i.e., Citrus irrigation recommendation, Department of Agricultural and Food, Government of Western Australia), orange trees irrigated by micro-irrigation system tend to have a shallow root systems.

The effective root-zone, of these trees, is usually the top 0.3 to 0.4 m, depending on soil type. Sweet orange [*Citrus sinensis* (L.) Pers.] cv. Mosambi aged 8 years budded on Rangpur lime (*C. limonia* Osbeck) was found to be a surface feeder with bulk of the active roots (70-90%) located in the top 0.3 m layer of soil during different seasons. The maximum root activity (65-81%) was confined to radial distance of 1.2 m (Kotur et al., 1998). The amount of water that can be held in the root zone varies with the type of irrigation system used, soil type, depth of effective root zone and proportion of stone or gravel in the soil.

The resistivity changes could be related to the different responses of the active roots in function of irrigation type and operations. Changes in the intensity of root activity and its pattern of distribution caused by variations in SWC in soil profile and shoot-growth activity, especially during the late rainy season and summer respectively (Kotur et al., 1998).

Variability in SWC changes in both vertical and lateral directions is likely due to root distribution and preferential pathways toward the roots with decreases in ground electrical conductivity and SWC due to drying of the soil during the RWU (Mares et al., 2016).

Chapter 5

Summary and conclusions

Summary and conclusions

This Chapter summarizes the main PhD Thesis findings and contributions, points out limitations of the current work, and outlines directions for future research.

The novelty and strong point of the PhD Thesis was the adoption of an integrated approach based on geophysical methods coupled with other measurements (micrometeorological ET and sap-flow fluxes measurements) in order to help solving the complexity of the SPAC interactions, specifically concerning RWU of orange trees in Mediterranean climate.

The state-of-the-art about SPAC monitoring includes numerous stand-alone methodologies (Chapter 2). As reported by scientific literature (Chapters 1 and 2), near-surface geophysics is strongly affected by both static and dynamic related to soil-subsoil characteristics and interactions with vegetation. This fact, if properly recognized, is potentially full of information on the soil-subsoil structure and behaviour. Our integrated approach has documented that the information is maximized when geophysical data are collected in time-lapse mode (short-term repetitions) and coupled with other measurements.

In particular, our experimental results have demonstrated that small scale 3-D ERT in time-lapse, combined with micrometeorological data, sap flow measurements and soil hydraulic characteristics is capable to characterize the pathways of water distribution and provides spatial

information on root-zone suction regions of irrigated orange trees (Chapter 3), also treated by deficit irrigation techniques (Chapter 4).

In Case study 1 (Chapter 3), the volume of soil affected by the RWU activity has been characterized by the 3-D ERT measurements coupled with tree transpiration measurements and micrometerological data. The information contained in the ERT measurements in terms of soil moisture changes was exploited by comparing the field results against a 1-D vadose zone model. The result of this approach (Case study 1, Chapter 3) has obvious consequences for the possible improvement of irrigation strategies, as it is apparent how the monitored orange tree essentially drives water from one to two drippers out of the four in total that should pertain to its area in the plantation. This means that it is very likely that half of the irrigated water was indeed lost to deeper layers and brings no contribution to the tree.

At Case study 2 (Chapter 4), time-lapse 3-D ERT monitoring (i.e., short-term repetitions within the 3D-ERT long-term monitoring within the irrigation season in 2015) was adopted with the purpose of assessing the electrical resistivity changes within the SP interface of different water-supplied orange trees (i.e. fully and deficit irrigated). Within the root-zone, a heterogeneous changing pattern of electrical resistivity was found in the two irrigation treatments. Variability in electrical resistivity in both vertical and lateral directions was likely due to root distribution and preferential water pathways toward the roots and/or bypassing the roots to percolate to deeper zones. Although changes in transpiration rates were

not explicitly determined from the ERT images, the technique can capture the timing of the resistivity change in the spatio-temporal variability of the subsoil around the trees, especially at the short-term scale.

Some limitations remain in the interpretation of ERT data at field scale. The effect of tree roots on soil electrical resistivity sometimes was difficult to discuss given the complexity of root-soil interactions, in this sense further investigations are needed. Moreover, the relationship between measured electrical resistivity and soil moisture is not always easy to calibrate. In fact, soil structure and constitution, temperature and root tissue may change the relationship and it remains difficult to quantify their influence. Careful calibration under well-known conditions still remains necessary.

Due to the complexity and heterogeneity of the studied sub-soil systems, the integration of hydrological and geophysical modelling may allow the explanation of the processes related to infiltration front (irrigation) and RWU (tree transpiration) processes. A complete exploitation of the obtainable information can be carried through appropriate modelling processes combining all available data (e.g. geophysical, data, micrometeorological data, hydrological data, etc.). In this sense our hydro-geophysical analyses represent an initial step toward constructing a hydrological concept model or a source of data for more sophisticate analyses including ERT into model describing the movement of water in the vadose zone (Hinnel et al., 2010).

With this PhD work, more advanced uses of geophysical data are now considered in combination with other measurements, especially linking soil moisture distribution with plant physiological response (i.e., transpiration fluxes) and active root distribution in the soil.

Long-run studies of this type may give a fundamental contribution to our understanding of SPAC interactions also in view of the facing challenges coming from climatic changes.

References

Aiello, R., Bagarello, V., Barbagallo, S., Consoli, S. Di Prima, S., Giordano, G., Iovino, M., 2014, An assessment of the Beerkan method for determining the hydraulic properties of a sandy loam soil. Geoderma, 235–236 (2014) 300–307

Al Hagrey, S. A. (2007). Geophysical imaging of root-zone, trunk, and moisture heterogeneity. Journal of Experimental Botany, 58(4), 839–854. http://doi.org/10.1093/jxb/erl237

Allen, R. G., Pereira, L. S., Raes, D., & Smith, M. (1998). Crop evapotranspiration: Guidelines for computing crop requirements. Irrigation and Drainage Paper No. 56, FAO, (56), 300. http://doi.org/10.1016/j.eja.2010.12.001

Allen, R.G., Pruitt, W.O., Wright, J.L., Howell, T.H., Ventura, F., Snyder, R., Itenfisu, D., Steduto, P., Berengena, J., Baselga Yrisarry, J., Smith, M., Pereira, L.S., Raes, D., Perrier, A., Alves, I., and Walter, I. (2006). A recommendation on standardized surface resistance for hourly calculation of reference ETo by the FAO56 Penman-Monteith method. Agricultural Water Management, 81, 1-2

Allred, B. J., Daniels, J. J., & Ehsani, M. R. (2008). Agricultural Geophysics. Water, xxii, 410. Retrieved from http://books.google.com/books?hl=en&lr=&id=4SDgk7xGZeQC&oi=fnd&pg=PR13&dq=Handbook+of+Agricultural+Geophysics&ots=U3fr6YZuAE&sig=lcRk8m9xIl_mIAYlWo3z-k0naGM

Amato, M., Basso, B., Celano, G., Bitella, G., Morelli, G., & Rossi, R. (2008). In situ detection of tree root distribution and biomass by multi-electrode resistivity imaging. Tree Physiology, 28(Pollen 2007), 1441–1448. http://doi.org/10.1093/treephys/28.10.1441

Amato, M., Rossi, R., Bitella, G., and Lovelli, S. (2010). Multielectrode

Geoelectrical Tomography for the Quantification of Plant Roots, Italian Journal of Agronomy, 3, 257–263

Archie, G.E. 1942. The electrical resistivity log as an aid in determining some reservoir characteristics. Trans. AIME 146:54–67

Aubinet, M, Grelle, A, Ibrom, A, Rannik, U, Moncrieff, J., Foken, T., Kowalski, P., Martin, P., Berbigier, P., Bernhofer, C., Clement, R., Elbers, J., Granier, A., Grunwald, T., Morgenster, K., Pilegaard, K., Rebmann, C., Snijders, W., Valentini, R., Vesala, T., 2000, Estimates of the annual net carbon and water exchange of Europeran forests: the EUROFLUX methodology, Adv.Ecol.Res. 30: 113-75

Aubrecht L., Stanik Z., Koller J. (2006). Electrical measurement of the absorption surfaces of tree roots by the earth impedance method: 1. Theory. Tree Physiology, 26:1105-1112

Beff, L., Gunther, T., Vandoorne, B., Couvreur, V., & Javaux, M. (2013). Three-dimensional monitoring of soil water content in a maize field using Electrical Resistivity Tomography. Hydrology and Earth System Sciences, 17(2), 595–609. http://doi.org/10.5194/hess-17-595-2013

Binley, A., Ramirez, A., Daily, W. (1995) Regularised image reconstruction of noisy electrical resistance tomography data. In: Beck MS, Hoyle BS, Morris MA, Waterfall RC, Williams RA (eds), Process tomography. Proceedings of the 4th Workshop of the European Concerted Action on Process Tomography, Bergen, 6–8, April 1995, pp. 401– 410

Binley, A., Henry-Poulter, S., & Shaw, B. (1996). Examination of Solute Transport in an Undisturbed Soil Column Using Electrical Resistance Tomography. Water Resources Research, 32(4), 763–769. http://doi.org/10.1029/95WR02995

Binley A.M., G. Cassiani, R. Middleton, and P., Winship, (2002). Vadose zone flow model parameterisation using cross-borehole radar and

resistivity imaging, Journal of Hydrology, 267, 147-159

Binley, A., & Kemna, A. (2005). DC Resistivity and Induced Polarization Methods. In Hydrogeophysics (pp. 129–156). Dordrecht: Springer Netherlands. http://doi.org/10.1007/1-4020-3102-5_5

Binley, A., Cassiani, G., Deiana, R., (2011): Hydrogeophysics – Opportunities and Challenges, Bollettino di Geofisica Teorica ed Applicata, 51(4), 267-284

Binley,A. (2014) R3 package http://www.es.lancs.ac.uk/people/amb/Freeware/freeware.htm (last access: December 2015)

Binley, A., S. S. Hubbard, J. A. Huisman, A. Revil, D. A. Robinson, K. Singha, and L. D. Slater (2015a), The emergence of hydrogeophysics for improved understanding of subsurface processes over multiple scales, Water Resour. Res., 51, 3837–3866, doi:10.1002/2015WR017016

Binley, A. (2015b). Tools and Techniques: Electrical Methods, In Treatise on Geophysics (Second Edition), edited by Gerald Schubert,, Elsevier, Oxford, 2015, Pages 233-259

Bitella, G., Rossi, R., Loperte, A., Satriani, A., Lapenna, V., Perniola, M., & Amato, M. (2015). Geophysical techniques for plant, soil, and root research related to sustainability. In The Sustainability of Agro-Food and Natural Resource Systems in the Mediterranean Basin (pp. 353-372). Springer International Publishing

Blum, A., (2011): Plant Water Relations, Plant Stress and Plant Production. In: Plant Breeding for Water-Limited Environments. Ed: Springer New York, pp 11-52

Boaga, J., Rossi, M., & Cassiani, G. (2013). Monitoring Soil-plant Interactions in an Apple Orchard Using 3D Electrical Resistivity Tomography. Procedia Environmental Sciences, 19, 394–402. http://doi.org/10.1016/j.proenv.2013.06.045

Brillante, L., Mathieu, O., Bois, B., van Leeuwen, C., & Lévêque, J. (2015). The use of soil electrical resistivity to monitor plant and soil water relationships in vineyards. Soil, 1(1), 273–286. http://doi.org/10.5194/soil-1-273-2015

Brotzge J. A., Crawford K. C., 2003. Examination of the Surface Energy Budget: A Comparison of Eddy Correlation and Bowen Ratio Measurement Systems. J. Hydrometeorol., 4, 160-178

Brovelli A. and G. Cassiani, 2011, Combined estimation of effective electrical conductivity and permittivity for soil monitoring, Water Resources Research, 47, W08510, doi:10.1029/2011WR010487, 2011

Burgess, S. S., Adams, M. A., Turner, N. C., & Ong, C. K. (1998). The redistribution of soil water by tree root systems. Oecologia, 115(3), 306-311

Cammalleri, C., Rallo, G., Agnese, C., Ciraolo, G., Minacapilli, M., & Provenzano, G. (2013). Combined use of eddy covariance and sap flow techniques for partition of ET fluxes and water stress assessment in an irrigated olive orchard. Agricultural Water Management, 120, 89–97. http://doi.org/10.1016/j.agwat.2012.10.003

Carminati, A., Vetterlein, D., Weller, U., Vogel, H. J., Oswald, S. E. (2009). When roots lose contact Vadose Zone J. 8 (2), 805-809, http://dx.doi.org/10.2136/vzj2008.0147

Carminati, A., Vetterlein, D., (2012): Plasticity of rhizosphere hydraulic properties as a key for efficient utilization of scarse resources. Ann. Bot. (Lond.) 112(2):277-290

Cassiani, G., Bruno, V., Villa, A., Fusi, N., and Binley, A. M. (2006). A saline trace test monitored via time-lapse surface electrical resistivity tomography, J. Appl. Geophys., 59, 244–259

Cassiani, G., Kemna, A., Villa, A., and Zimmermann, E. (2009). Spectral

induced polarization for the characterization of freephase hydrocarbon contamination in sediments with low clay content, Near Surface Geophysics, special issue on Hydrogeophysics – Methods and Processes, 547–562, doi:10.3997/1873-0604.2009028

Cassiani G., N. Ursino, R. Deiana, G. Vignoli, J. Boaga, M. Rossi, M. T. Perri, M. Blaschek, R. Duttmann, S. Meyer, R. Ludwig, A. Soddu, P. Dietrich and U. Werban (2012). Non-invasive monitoring of soil static characteristics and dynamic states: a case study highlighting vegetation effects, Vadose Zone Journal, Special Issue on SPAC - Soil-plant interactions from local to landscape scale, August 2012, V.11, vzj2011.0195, doi: 10.2136/2011.0195

Cassiani, G., Boaga, J., Vanella, D., Perri, M. T., & Consoli, S. (2015). Monitoring and modelling of soil-plant interactions: The joint use of ERT, sap flow and eddy covariance data to characterize the volume of an orange tree root zone. Hydrology and Earth System Sciences, 19(5), 2213–2225. http://doi.org/10.5194/hess-19-2213-2015

Cassiani, G., Ursino, N., Deiana, R., Vignoli, G., Boaga, J., Cassiani, G., Boaga, J., Rossi, M., Putti, M., Fadda, G., Majone, B., & Bellin, A. (2016). Soil-plant interaction monitoring: Small scale example of an apple orchard in Trentino, North-Eastern Italy. Science of the Total Environment, 543, 851–861. http://doi.org/10.1016/j.scitotenv.2015.03.113

Castellví, F., Consoli, S. and Papa, R. 2012, Sensible heat flux estimates using two different methods based on Surface renewal analysis. A study case over an orange orchard in Sicily. Agri. Forest Meteorol. 152:58-64

Cohen Y., Fuchs M., Green G. C., 1981. Improvement of the heat-pulse method for determining sap flow in trees. Plant Cell Environ., 4, 391-397

Consoli, S., Licciardello, F., Vanella, D., Pasotti, L., Villani, G., & Tomei, F. (2016 a). Testing the water balance model criteria using TDR

measurements, micrometeorological data and satellite-based information. Agricultural Water Management, 170, 68–80

Consoli, S., Papa, R., (2013). Corrected surface energy balance to measure and model the evapotranspiration of irrigated orange orchards in semi-arid Mediterranean conditions. Irrigation Science September 2013, Volume 31, Issue 5, pp 1159-1171

Consoli S., Stagno F., Roccuzzo G., Cirelli G. Intrigliolo F. (2014). Sustainable management of limited water resources in a young orange orchard. Agricultural Water Management, Vol. 132, pp. 60-68

Consoli S, Stagno F, Vanella D, Boaga J, Cassiani G, Roccuzzo G (2016 b). Partial root-zone drying irrigation for orange orchards: effects on water use and crop production characteristics. In press, European Journal of Agronomy

Consoli, S., & Vanella, D. (2014 a). Comparisons of satellite-based models for estimating evapotranspiration fluxes. Journal of Hydrology, 513, 475–489

Consoli, S., & Vanella, D. (2014 b). Mapping crop evapotranspiration by integrating vegetation indices into a soil water balance model. Agricultural Water Management, 143, 71-81

Constable, S., R. Parker and C. Constable, (1987). Occam's inversion: A practical algorithm for generating smooth models from electromagnetic sounding data, Geophysics, 52(3), 289–300

Council, N. R. (2004). Valuing Ecosystem Services. Washington, D.C.: National Academies Press. http://doi.org/10.17226/11139

Couvreur, V., Vanderborght, J., Javaux, M. (2012): A simple three-dimensional macroscopic root water uptake model based on the hydraulic architecture approach. Hydrol. Earth Syst. Sci., 16, 2957–2971. doi:10.5194/hess-16-2957-2012

Daily, W.A., Ramirez, A., Binley, A., LaBrecque, D., (2004). Electrical resistivity tomography. Leading Edge 23 (5), 438–442

deGroot-Hedlin, C., Constable, S., (1990). Occam's inversion to generate smooth, twodimensional models from magnetotelluric data. Geophysics 55–12, 1613–1624

Deiana R., G. Cassiani, A. Kemna, A. Villa, V. Bruno and A.Bagliani, (2007). An experiment of non invasive characterization of the vadose zone via water injection and cross-hole time-lapse geophysical monitoring, Near Surface Geophysics, Vol 5, 3 June 2007, 183-194, doi: 10.3997/1873-0604.2006030

Doolittle, J., Petersen, M., & Wheeler, T. (2001). Comparison of two electromagnetic induction tools in salinity appraisals. Journal of Soil and Water Conservation, 56(3), 257-262

Doussan, C ., Pierret, A., Garrigues, E., Pagès, L., (2006) Water uptake by plant roots: II – Modelling of water transfer in thesoil root-system with explicit account of flow within the root system – Comparison with experiments. Plant and Soil (2006) 283:99–117. DOI 10.1007/s11104-004-7904-z

Drexler, J. Z., Snyder, R. L., Spano, D., Paw, U., & Tha, K. (2004). A review of models and micrometeorological methods used to estimate wetland evapotranspiration. Hydrological Processes, 18(11), 2071-2101

Du, C., & Zhou, J. (2009). Evaluation of soil fertility using infrared spectroscopy: A review. Environmental Chemistry Letters, 7(2), 97–113. http://doi.org/10.1007/s10311-008-0166-x

Feddes, R. A., Hoff, H., Bruen, M., Dawson, T., de Rosnay, P., Dirmeyer, P., Jackson, R. B., Kabat, P., Kleidon, A., Lilly, A., and Pitman, A. J.: Modelling Root Water Uptake in Hydrological and Climate Models, B. Am. Meteor. Soc., 82, 2797–2809, 2001

Friedman, S.P., 2005. Soil properties influencing apparent electrical

conductivity: a review. Computers and Electronics in Agriculture 46, 45–70

Foken T., (2008). Micrometeorology. Springer-Verlag, Berlin Heidelberg, 306 pp.

Garré, S., Javaux, M., Vanderborght, J., Pagès, L., Vereecken, H., (2011). Three-Dimensional Electrical Resistivity Tomography to Monitor Root Zone Water Dynamics. Vadose Zone Journal 10(1):412-424. DOI: 10.2136/vzj2010.0079

Garré, S., Günther, T., Diels, J., & Vanderborght, J. (2012). Evaluating experimental design of ERT for soil moisture monitoring in contour hedgerow Iintercropping systems. Vadose Zone Journal, 11(4), 0. http://doi.org/10.2136/vzj2011.0186

Geuzaine, C., & Remacle, J. F. (2009). Gmsh: A 3-D finite element mesh generator with built-in pre-and post-processing facilities. International Journal for Numerical Methods in Engineering, 79(11), 1309-1331

Göckede M., Rebmann C., Foken T., 2004. A combination of quality assessment tools for eddy covariance measurements with footprint modelling for the characterisation of complex sites. Agric. Forest Meteorol., 127, 175-188

Gong, D., Shaozhong, K., Zhang, L., Taisheng, D., Limin, Y., (2006): A two-dimensional model of root water uptake for single apple trees and its verification with sap flow and soil water content measurements. Agricultural Water Management 83:119–129

Green S., (2009). Measurements of Sap Flow by the Heat-Pulse Method. An instruction manual for the HPV system. New Zeland.

Green, S. R., Vogeler, I., Clothier, B. E., Mills, T. M., van den Dijssel, C., (2003a): Modelling water uptake by a mature apple tree. Australian Journal Of Soil Research, 41: 365-380

Green, S., Clothier, B., Jardine B., (2003b): Theory and Practical Application of Heat Pulse to Measure Sap Flow. Agronomy Journal; Nov/Dec 2003; 95, 6; ProQuest Agriculture Journals pg. 1371

Grote, K., Hubbard, S., & Rubin, Y. (2003). Field-scale estimation of volumetric water content using ground-penetrating radar ground wave techniques. Water resources research, 39(11)

Hendrickx, J. M. H., Baerends, B., Raza, Z. I., Sadig, M., & Chaudhry, M. A. (1992). Soil salinity assessment by electromagnetic induction of irrigated land. Soil Science Society of America Journal, 56(6), 1933-1941.

Hinnel, A.C., Ferré, T.P.A., Vrugt, J.A., Huisman, J.A., Moysey, S., Rings, J., Kowalsky, M.B., (2010). Improved extraction of hydrological information from geophysical data through coupled hydrogeophysical inversion. Water resources research, 46(4)

Hose, E., Steudle, E., Hartung, W., (2000): Abscisic acid and hydraulic conductivity of maize roots: a study using cell- and root-pressure probes. Plant Soil 321(1–2):153–187

Huang, J., Scudiero, E., Choo, H., Corwin, D. L., & Triantafilis, J. (2016). Mapping soil moisture across an irrigated field using electromagnetic conductivity imaging. Agricultural Water Management, 163, 285-294

Jarvis, N.J., (1989): A simple empirical-model of root water-uptake. J. Hydrol. 107(1–4):57–72. doi:10.1016/0022-1694(89)90050-4

Jarvis, N.J., (2011): Simple physics-based models of compensatory plant water uptake: concepts and eco-hydrological consequences. J. Hydrol. 15, 3431–3446. doi:10.5194/hess-15-3431-2011

Javaux, M., Couvreur, V., Vanderborght, J., & Vereecken, H. (2013). Root water uptake: from three-dimensional biophysical processes to macroscopic modeling approaches. Vadose Zone Journal, 12(4)

Javaux, M., Schröder, T., Vanderborght, J., & Vereecken, H. (2008). Use of a Three-Dimensional Detailed Modeling Approach for Predicting Root Water Uptake. Vadose Zone J., 7(3), 1079–1088. http://doi.org/10.2136/vzj2007.0115

Jayawickreme, D. H., Jobbagy, E. G., & Jackson, R. B. (2014). Geophysical subsurface imaging for ecological applications. New Phytologist, 201(4), 1170–1175. http://doi.org/10.1111/nph.12619

Jayawickreme, D. H., van Dam, R. L., & Hyndman, D. W. (2008). Subsurface imaging of vegetation, climate, and root-zone moisture interactions. Geophysical Research Letters, 35(18), 1–5. http://doi.org/10.1029/2008GL034690

Jones, H. G. and Tardieu, F. (1998). Modelling water relations of horticultural crops: a review, Sci. Hortic.-Amsterdam, 74, 21–46

Kaimal, J.C., Finnigan, J., 1994, Atmospheric Boundary Layer Flows: Their Structure and Measurement. Oxford University Press, New York, pp. 255–261

Katerji N., Rana G., 2008. Crop evapotranspiration measurements and estimation in the Mediterranean region. CRA-SCA, Bari, 173 pp

Kluitenberg G. J., Ham J. M., 2004. Improved theory for calculating sap flow with the heat pulse method. Agric. Forest Meteorol., 126, 169-173

Koestel J., A. Kemna, M. Javaux, A. Binley and H. Vereecken, 2008, Quantitative imaging of solute transport in an unsaturated and undisturbed soil monolith with 3-D ERT and TDR, Water Resour. Res., 44, W12411, doi:10.1029/2007WR006755

Kotur, S. C., & Keshava Murthy, S. V. (1998). Root activity distribution studies in citrus, grape, mango and guava using isotopic techniques. Karnataka Journal of Agricultural Science, 11, 651-657

Lin, H. (2010). Earth ' s Critical Zone and hydropedology : concepts ,

characteristics , and advances, 25–45.

Lin, H.J., Richards, D.R., Talbot, C.A., Yeh, G.-T., Cheng, J., Cheng, H., 1997. FEMWATER: a three-dimensional finite element computer model for simulating density-dependent flow and transport in variably saturated media. US Army Corps of Engineers and Pennsylvania State University Technical Report CHL-97-12.

Lin, H. S., Mcdonnell, J. J., Nimmo, J. R., & Pachepsky, Y. A. (2015). Hydropedology: Synergistic integration of soil science and hydrology in the Critical Zone. Hydrological Processes, 29(21), 4559–4561. http://doi.org/10.1002/hyp.10686

Lunt, I. A., Hubbard, S. S., & Rubin, Y. (2005). Soil moisture content estimation using ground-penetrating radar reflection data. Journal of Hydrology, 307(1), 254-269

Mancuso, S., (2012). Measuring Roots: An Updated Approach. Springer Science & Business Media, 382 pages

Mares, R., Barnard, H. R., Mao, D., Revil, A., & Singha, K. (2016). Examining diel patterns of soil and xylem moisture using electrical resistivity imaging. Journal of Hydrology, 536, 327-338

Marshall D.C., 1958. Measurement of sap flow in conifers by heat transport. Plant Physiol., 33, 385-396

Mauder, M. and Foken, T. (2004). Documentation and instruction manual of the eddy covariance software package TK2. Universität Bayreuth, Abt. Mikrometeorologie, Arbeitsergebnisse, http://www.geo.unibayreuth.de/mikrometeorologie/ARBERG, pp. 26-44

Mauder, M., Oncley, S. P., Vogt, R., Weidinger, T., Ribeiro, L., Bernhofer, C., Foken, T., Kosiek, W., De Bruin, H. A. R. and Liu, H. (2007). The energy balance experiment EBEX-2000. Part II. Intercomparison of eddy-covariance sensors and post-field data processing methods. Bound.-Layer Meteorol. 123

doi:10.1007/s10546-006-9139-4

Mauder M., Desjardins R. L., Pattey E., Worth D. (2010). An Attempt to Close the Daytime Surface Energy Balance Using Spatially-Averaged Flux Measurements. Bound.-Layer Meteorol., 136, 175-191

Michot, D., Benderitter, Y., Dorigny, A., Nicoullaud, B., King, D.,and Tabbagh, A., (2003). Spatial and temporal monitoring of soil water content with an irrigated corn crop cover using surface electrical resistivity tomography. Water Resources Research, 39(5), 1–20. http://doi.org/10.1029/2002WR001581

Minacapilli, M., Consoli, S., Vanella, D., Ciraolo, G., & Motisi, A. (2016). A time domain triangle method approach to estimate actual evapotranspiration: Application in a Mediterranean region using MODIS and MSG-SEVIRI products. Remote Sensing of Environment, 174, 10-23

Moncrieff, J.B., Clement, R., Finnigan, J.J. and Meyers, T., 2004, Averaging and de-trending. Handbook of Micrometeorology. Lee, X., Massman, W. and Law, B. (Eds) Kluwer Acad. Publ., Chapter 2, pp 7-31.

Monego, M., Cassiani, G., Deiana, R., Putti, M., Passadore, G., and Altissimo, L. (2010). Tracer test in a shallow heterogeneous aquifer monitored via time-lapse surface ERT, Geophysics, 75, WA61–WA73, doi:10.1190/1.3474601

Moreno, Z., Arnon, A., & Furman, A. (2015). Hydro-geophysical monitoring of orchard root zone dynamics in semi-arid region. Irrigation Science, 33, 303–318. http://doi.org/10.1007/s00271-015-0467-3

Motisi, A., Consoli, S., Rossi, F., Minacapilli, M., Cammalleri, C. Papa, R., Rallo, G., D'Urso G. (2012). Eddy covariance and sap flow measurements of energy and mass exchange of woody crops in a Mediterranean environment. Acta Horticolturae 951, 121-127

Musters, P. A. D., Bouten, W., (2000): A method for identifying optimum strategies of measuring soil water contents for calibrating a root water uptake model. J. Hydrol, 227:273-286

Nijland, W., van der Meijde, M., Addink, E. A., & de Jong, S. M. (2010). Detection of soil moisture and vegetation water abstraction in a mediterranean natural area using electrical resistivity tomography. Catena, 81(3), 209–216. http://doi.org/10.1016/j.catena.2010.03.005

Paglis, C. M. (2013). Application of electrical resistivity tomography for detecting root biomass in coffee trees. International Journal of Geophysics, 2013(1). http://doi.org/10.1155/2013/383261

Parasnis D.S., 1988. Reciprocity theorems in geoelectric and geoelectromagnetic work, Geoexploration, 25, 177–198

Parsekian, A. D., Singha, K., Minsley, B. J., Holbrook, W. S., & Slater, L. (2015). Multiscale geophysical imaging of the critical zone. Reviews of Geophysics, 53(1), 1-26

Philip, J. R. (1966). Plant water relations: some physical aspects. Annual Review of Plant Physiology, 17(1), 245–268. http://doi.org/10.1146/annurev.pp.17.060166.001333

Raats, P. A. C.: Uptake of water from soils by plant roots, Transp.

Porous. Med., 68, 5–28, 2007Rhoades, J. D., & Ingvalson, R. D. (1971). Determining salinity in field soils with soil resistance measurements. Soil Science Society of America Journal, 35(1), 54-60

Rana, G, Katerji, N., (2000). Measurement and estimation of actual evapotranspiration in the field under Mediterranean climate: a review. European Journal of Agronomy 13, 125-153

Rhoades, J. D., Kandiah, A., & Mashali, A. M. (1992). The use of saline waters for crop production (Vol. 48). Rome: FAO

Robinson, D. A., Campbell, C. S., Hopmans, J. W., Hornbuckle, B. K., Jones, S. B., Knight, R., Ogden, F., Selker, J., Wendroth, O. (2008). Soil moisture measurement for ecological and hydrological watershed-scale observatories: A review. Vadose Zone Journal, 7(1), 358-389

Robinson, J. L., Slater, L. D., & Schäfer, K. V. R. (2012). Evidence for spatial variability in hydraulic redistribution within an oak-pine forest from resistivity imaging. Journal of Hydrology, 430–431, 69–79. http://doi.org/10.1016/j.jhydrol.2012.02.002

Romano, N. (2014). Soil moisture at local scale: Measurements and simulations. Journal of Hydrology, 516, 6-20

Rossi, R. Amato, M., Bitella, G., Bochicchio, R., Ferreira Gomes, J., J., Lovelli, S., Martorella, E., Favale, P., (2011). Electrical resistivity tomography as a non-destructive method for mapping root biomass in an orchard. European Journal of Soil Science, 62 (2), 206–215

Rubin Y. and Hubbard S.S. (eds), (2005): Hydrogeophysics. Springer, Dordrecht, 523 pp

Samouëlian, A., Cousin, I., Tabbagh, A., Bruand, A., & Richard, G. (2005). Electrical resistivity survey in soil science: A review. Soil and Tillage Research, 83(2), 173–193. http://doi.org/10.1016/j.still.2004.10.004

Satriani, A., Loperte, A., Soldovieri, F., (2015). Integrated geophysical techniques for sustainable management of water resource. A case study of local dry bean versus commercial common bean cultivars, Agricultural Water Management, 162, 57-66

Schneider, C. L., Attinger, S. , Delfs, J.-O., Hildebrandt, A. (2010): Implementing small scale processes at the soil-plant interface – the role of root architectures for calculating root water uptake profiles. Hydrol. Earth Syst. Sci., 14, 279–289, 2010

Schwartz, B. F., Schreiber, M. E., & Yan, T. (2008). Quantifying field-

scale soil moisture using electrical resistivity imaging. Journal of Hydrology, 362(3–4), 234–246. http://doi.org/10.1016/j.jhydrol.2008.08.027

Shanahan, P., A. Binley, R. Whalley and C. Watts, 2015, The Use of Electromagnetic Induction to Monitor Changes in Soil Moisture Profiles beneath Different Wheat Genotypes, Soil Science Society of America Journal, 79(2), 459-466

Shea, P. F., & Luthin, J. N. (1961). An investigation of the use of the four-electrode probe for measuring soil salinity in situ. Soil Science, 92(5), 331-339

Sheets, K. R., & Hendrickx, J. M. (1995). Noninvasive soil water content measurement using electromagnetic induction. Water resources research, 31(10), 2401-2409

Si J, Feng Q, Xi H, Chang Z, Su Y, Zhang K (2009) Sap-flow measurement and scale transferring from sample trees to entire forest stand of Populus euphratica in desert riparian forest in extreme arid region. Sciences in Cold and Arid Regions, 1(3), 258-266

Slater, L. and A. Binley, 2006, Synthetic and field based electrical imaging of a zerovalent iron barrier: Implications for monitoring long-term barrier performance, Geophysics, 71 (5), B129-B137

Smith M., Allen R. G. (1996). Measurement of sap flow in plant stems. Journal of Experimental Botany, Vol. 47, No. 305, pp. 1833-1844

Smith M., Allen R. G., Monteith J. L., Perrier A., Pereira L. S., Segeren A., (1991). Report on the expert consultation on revision of FAO methodologies for crop water requirements. FAO Land and Water Development Division, FAO, Rome, 129 pp

Spank U., Bernhofer C., (2008). Another Simple Method of Spectral Correction to Obtain Robust Eddy-Covariance Results. Bound.-Layer Meteorol., 128, 403-422

Srayeddin, I., & Doussan, C. (2009). Estimation of the spatial variability of root water uptake of maize and sorghum at the field scale by electrical resistivity tomography. Plant and Soil, 319(1–2), 185–207. http://doi.org/10.1007/s11104-008-9860-5

Stull, R. B. (1988). An introduction to boundary layer meteorology. In: Atmosperic Science Library, Kluwer, Dordrechr, The Netherlands, p. 666

Swanson, R.H. and Whitfield, D.W. (1981). A numerical analysis of heat pulse velocity theory and practice. J. Exp. Bot. 32:221-239

Tenhunen, J. D., Catarino, F. M., Lange, O. L., & Oechel, W. C. (Eds.), (2013). Plant response to stress: functional analysis in mediterranean ecosystems (Vol. 15). Springer Science & Business Media

Tikhonov, A. N., and V. Y. Arsenin, 1977, Solutions of ill-posed problems, John Wiley and Sons, Inc

Ursino N., G. Cassiani, R. Deiana, G. Vignoli and J. Boaga, (2014), Measuring and Modelling water related soil – vegetation feedbacks in a fallow plot, Hydrology and Earth System Sciences (HESS), doi:10.5194/hess-18-1105-2014

van den Honert, T. H. (1948). Water transport in plants as a catenary process. Discussions of the Faraday Society, 3, 146-153

van Genuchten, M. T., 1980, A closed form equation for predicting the hydraulic conductivity of unsaturated soils. Soil Sci. Soc. Am. J. 44: 892–898

Vanella, D. Consoli, S., Cassiani, G., Busato, L., Boaga, J, Barbagallo, S., Binley, A, (2016). The use of small scale electrical resistivity tomography to identify trees root water uptake patterns. Submitted to Journal of Hydrology

Vereecken H, Binley A, Cassiani G, Kharkhordin I, Revil A, Titov K.,

(2006), Applied Hydrogeophysics, Springer-Verlag, Berlin (eds)

Vereecken, H., Huisman, J. A., Bogena, H., Vanderborght, J., Vrugt, J. A., & Hopmans, J. W. (2008). On the value of soil moisture measurements in vadose zone hydrology: A review. Water resources research, 44(4)

Waxman M. H., Smits L. J. M., (1968): Electrical conductivities in oil-bearing shaly sands, Soc. Petr. Eng. J., 8, 107–122

Werban, U., Attia al Hagrey, S., & Rabbel, W. (2008). Monitoring of root-zone water content in the laboratory by 2D geoelectrical tomography. Journal of Plant Nutrition and Soil Science, 171(6), 927-935

Wilding, L. P., & Lin, H. (2006). Advancing the frontiers of soil science towards a geoscience. Geoderma, 131(3–4), 257–274. http://doi.org/10.1016/j.geoderma.2005.03.028

Wilson, K. B., Goldstein, A. H., Falge, E., 2002, Energy balance closure at FLUXNET sites. Agriculture and Forest Meteorology, 113, 223-243

Zhou, Q. Y., Shimada, J., & Sato, A. (2001). Measurement in lab, 37(2), 273–285

Zimmermann, E., Kemna, A., Berwix, J., Glaas,W., Münch, H. M., and Huisman, J. A.: A high-accuracy impedance spectrometer for measuring sediments with low polarizability, Meas. Sci. Technol., 19, 105603, doi:10.1088/0957-0233/19/10/105603, 2008